TECHNICAL PAPER

ISSN 1047-3289 *J. Air & Waste Manage. Assoc.* **56**:474–491
Copyright 2006 Air & Waste Management Association

Comparison of Continuous and Filter-Based Carbon Measurements at the Fresno Supersite

Kihong Park, Judith C. Chow, John G. Watson, Dana L. Trimble, and Prakash Doraiswamy
Desert Research Institute, Reno, NV

Kihong Park
Gwangju Institute of Science and Technology, Gwangju, Korea

W. Pat Arnott
University of Nevada, Reno, NV

Kenneth R. Stroud, Kenneth Bowers, and Richard Bode
California Air Resources Board, Sacramento, CA

Andre Petzold
Deutsches Zentrum fur Luft—und Raumfahrt Oberpfaffenhofen, Institut fur Physik der Atmosphare, Wessling, Germany

Anthony D.A. Hansen
Lawrence Berkeley National Laboratory, Berkeley, CA

ABSTRACT

Results from six continuous and semicontinuous black carbon (BC) and elemental carbon (EC) measurement methods are compared for ambient samples collected from December 2003 through November 2004 at the Fresno Supersite in California. Instruments included a multi-angle absorption photometer (MAAP; λ = 670 nm); a dual-wavelength (λ = 370 and 880 nm) aethalometer; seven-color (λ = 370, 470, 520, 590, 660, 880, and 950 nm) aethalometers; the Sunset Laboratory carbon aerosol analysis field instrument; a photoacoustic light absorption analyzer (λ = 1047 nm); and the R&P 5400 ambient carbon particulate monitor. All of these acquired BC or EC measurements over periods of 1 min to 1 hr. Twenty-four-hour integrated filter samples were also acquired and analyzed by the Interagency Monitoring of Protected Visual Environments (IMPROVE) thermal/optical reflectance carbon analysis protocol. Site-specific mass absorption efficiencies estimated by comparing light absorption with IMPROVE EC concentrations were 5.5 m^2/g for the MAAP, 10 m^2/g for the aethalometer at a wavelength of 880 nm, and 2.3 m^2/g for the photoacoustic analyzer; these differed from the default efficiencies of 6.5, 16.6, and 5 m^2/g, respectively. Scaling absorption by inverse wavelength did not provide equivalent light absorption coefficients among the instruments for the Fresno aerosol measurements. Ratios of light absorption at 370 nm to those at 880 nm from the aethalometer were nearly twice as high in winter as in summer. This is consistent with wintertime contributions from vehicle exhaust and from residential wood combustion, which is believed to absorb more shorter-wavelength light. To reconcile BC and EC measurements obtained by different methods, a better understanding is needed of the wavelength dependence of light-absorption and mass-absorption efficiencies and how they vary with different aerosol composition.

IMPLICATIONS

BC can be measured in situ and continuously by optical, thermal, and photoacoustic methods. The results of these measurements are highly correlated but have different absolute values. Relationships differ with changes in the sampled particles (e.g., winter vs summer). Both light- and mass-absorption efficiencies convert light absorption (i.e., the Angstrom Power Law [$\lambda^{-\alpha}$], assuming $\alpha = 1$) to BC, and both are wavelength dependent. The assumption that these efficiencies scale with inverse wavelength is not true at the Fresno Supersite and probably not at other locations.

INTRODUCTION

Black carbon (BC), or elemental carbon (EC), particles originate mostly from incomplete combustion of fuels and are major contributors to aerosol light absorption (b_{abs}, units of inverse megameters [Mm^{-1}]) in exhaust emissions and ambient air. Both BC and EC affect visibility, health, and the earth's radiation balance.[1–6] The terms BC, EC, light-absorbing carbon, and soot have been used interchangeably by many researchers, depending on the material sampled, the method used for quantification, and the uses of the data. This imprecise usage, coupled

with method-dependent definitions for BC or EC, has resulted in much confusion about their comparability.[5]

The most commonly used methods for determining BC and EC extract particles from the air onto a filter, followed by optical and/or thermal analyses.[5] In optical methods, the attenuation of light (b_{abs}) with wavelength (λ) reflected from, or transmitted through, the particle deposit relative to the blank filter is used to estimate $b_{abs}(\lambda)$. The $b_{abs}(\lambda)$ is divided by a mass absorption efficiency, $\sigma_{abs}(\lambda)$ (units of m^2/g), to obtain the BC concentration in $\mu g/m^3$. The wavelength dependence for b_{abs} and σ_{abs} is often scaled as λ^{-1}, following the Angstrom Power Law (λ^{α}) where $\alpha = 1$, but α depends on the chemical and physical properties of the sampled aerosol and the filter medium. Kirchstetter et al.[7] found that the λ^{-1} scaling approximated the behavior of fresh vehicle exhaust, but that a λ^{-2} scaling was more appropriate for biomass burning aerosol.

In addition to λ, light scattering in the filter medium, light-scattering particles deposited on the filter, and filter loading influence the accurate determination of BC concentrations.[6,8–10] Fuller et al.[11] and Martins et al.[12] applied advanced optical models to different particle compositions, sizes, and shapes to estimate σ_{abs} ranging from 2 to 30 m^2/g. Empirical measurements of σ_{abs} have been reported in a range of 2 to 17 m^2/g.[6,13] Bond and Bergstrom[14] suggested a σ_{abs}(550 nm) of 7.5 $\pm$ 1.2 m^2/g for freshly emitted particles.

In thermal methods for measuring EC, the filter is heated so that carbon evolves at specified temperatures in both nonoxidizing and oxidizing carrier gases. These methods are intended to separate organic carbon (OC) from EC. Carbonate carbon, typically in the form of calcite ($CaCO_3$), may also be classified as OC or EC at high temperatures (>800 °C), but it is found only when erosion of non-weathered crustal material is a large contributor to the sample.[15,16] Although EC will combust in an oxidizing atmosphere, it is stable at high temperatures (<700 °C) in inert atmospheres (e.g., helium [He]).

Some thermal methods use optical monitoring to correct for the charring of OC to EC in nonoxidizing atmospheres. Different temperature and charring-correction protocols have resulted in different values of EC even within the same thermal evolution method.[17,18] Currie et al.[19] found that the lowest and highest EC reported by different laboratories for the same standard filter sample differed by a factor of 7.

Photoacoustic detection[20–22] measures $b_{abs}(\lambda)$ on particles that have not been changed by filter collection. The photoacoustic analyzer draws particle-laden air into an acoustic resonator through which a high-intensity, modulated, monochromatic light beam is directed. A sound wave is produced at the modulation frequency by expansion of the air when particles absorb energy from light. Matching the modulation frequency to the resonator frequency reinforces the acoustic wave for measurement with a sensitive microphone; $b_{abs}(\lambda)$ is proportional to the sound energy, and particle absorption is divided by an empirically derived $\sigma_{abs}(\lambda)$ to attain a BC concentration.

Recent studies have compared and evaluated several current optical, thermal, and photoacoustic BC and EC measurement methods under controlled laboratory conditions.[23–26] Saathoff et al.[24] generated diesel soot, graphite electric arc soot, organic-coated soot, and mixtures of soot and ammonium sulfate during the Aerosols, Interactions and Dynamics in the Atmosphere (AIDA) soot aerosol campaign in 1999. They found that optical methods required different $\sigma_{abs}(\lambda)$ for diesel-soot and arc-soot aerosols to determine BC concentrations. The $\sigma_{abs}(\lambda)$ determined by optical techniques varied depending on the source type, wavelengths used, and measurement method. Schnaiter et al.[25] reported a σ_{abs}(450 nm) value of 10.6 m^2/g for diesel soot and 5.6 m^2/g for the graphite electric arc generator. The difference was attributed to different particle structures. These experiments showed higher a σ_{abs}(450 nm) for coated BC particles, similar to the theoretical findings of Fuller et al.[11] Sheridan et al.[26] used laboratory-generated diesel soot and kerosene and found reasonable agreements among (1) photoacoustic b_{abs}(532 nm); (2) the difference between particle light extinction and scattering; and (3) filter-based b_{abs}.

Watson et al.[5] summarized nearly 40 published intercomparison studies of optical, thermal, and photoacoustic measures of BC and EC. Some comparisons showed good agreement among the different methods, whereas others showed wide disagreements for the same methods applied to different samples. Agreement was typically better for laboratory-generated particles than for ambient air samples. Watson et al.[5] concluded that citation of a single BC or EC comparison study is insufficient to justify comparability among the different measurement methods. Lacking a more systematic understanding of the differences, aerosol- and instrument-specific comparisons are needed to use measurements interchangeably.

For this study, eight continuous or semicontinuous and integrated BC or EC measurement methods, as detailed in Table 1, were used to sample air at the Fresno Supersite.[27,28] In addition to these continuous and time-integrated carbon measurements, the Supersite provides continuous data of 1-hr or less for particle number concentration (3–407 nm), particle light scattering (b_{scat} [530 nm], units of Mm^{-1}), fine particulate matter ($PM_{2.5}$) mass, nitrate (NO_3^-), and gaseous nitrogen oxides (NO_x), carbon monoxide (CO), and ozone (O_3) that can be used to better understand differences among these BC and EC measurements. The analysis approach taken here can be applied at other sites that use similar measurements.

EXPERIMENTAL APPROACH

Fresno is located in California's San Joaquin Valley (SJV), which is in nonattainment of the $PM_{2.5}$ National Ambient Air Quality Standards. Air pollution in central California is affected by different types of emissions, including point sources (e.g., steam generators and natural gas combustion), area sources (e.g., residential wood combustion [RWC] and cooking), on-road and non-road mobile sources (e.g., gasoline- and diesel-fueled vehicles, high emitters, and cold starts in winter), agricultural sources (e.g., tillage, field burning, and fertilizers), and biogenic sources (e.g., plants and crops).[27] OC and EC are important components of $PM_{2.5}$ in the SJV,[29,30] and the relative abundances of OC and EC are used to evaluate source contributions for emission reduction strategies. The

Table 1. Summary of BC and EC measurement methods.

Instruments[a]	Observable (units)	Measurement Principle[b]	Wavelength (nm)	Inlet	Collection Medium	Flow Rate (L/min)	Averaging Time
MAAP	b_{abs} (Mm^{-1}) BC ($\mu g/m^3$)	Light reflected from the filter at 130° and 165° from the illumination direction are used in a radiative transfer model to estimate b_{abs} and is converted to BC using σ_{abs} of 6.5 m^2/g.	670	$PM_{2.5}$ cyclone	Glass-fiber filter tape	16	1 min
2-AE	b_{abs} (Mm^{-1}) BC ($\mu g/m^3$)	Attenuation of light transmitted through the filter tape is measured and converted to BC using σ_{abs} of 14,625/λ (m^2/g).	370,880	$PM_{2.5}$ cyclone	Quartz-fiber filter tape	6.8	5 min
7-AE	b_{abs} (Mm^{-1}) BC ($\mu g/m^3$)		370, 470, 520, 590, 660, 880, 950	$PM_{2.5}$ cyclone	Quartz-fiber filter tape	6.8	5 min
Photoacoustic	b_{abs} (Mm^{-1}) BC ($\mu g/m^3$)	Light absorption by particles in air results in heating of the surrounding air. The expansion of the heated air produces an acoustic (sound wave) signal that is detected by a microphone to determine b_{abs}, which is converted to BC using $\sigma_{abs} = 5$ m^2/g	1047	TSP[b]	Acoustic resonator	3	5 min
Sunset	OC, EC ($\mu g/m^3$)	Particles collected on a quartz-fiber filter are subjected to different temperature ramps following the NIOSH 5040 TOT protocol, and the resulting CO_2 is analyzed by NDIR. Pyrolysis correction is by laser transmittance.	660	$PM_{2.5}$ cyclone	Quartz-fiber filter tape	8.5	1 hr
	BC ($\mu g/m^3$)	Light transmitted through the filter is monitored during the collection phase to quantify BC.	660	$PM_{2.5}$ cyclone	Quartz-fiber filter tape	8.5	1 hr
R&P 5400	OC, EC, and TC ($\mu g/m^3$)	Particles collected on an impactor are heated to 275 °C for OC and to 750 °C for TC, and the resulting CO_2 is measured by NDIR. EC is obtained by the difference between TC and OC.	NA	$PM_{2.5}$ cyclone	Impactor	16.7	1 hr
PAS-PAH	Particle-bound PAH (fA)	The air stream is exposed to UV radiation, which ionizes the particle-bound PAH molecules. The charged particles are collected on a filter element, and the pizeoelectric current is proportional to the particle-bound PAH.	225	$PM_{2.5}$ impactor	Filter element mounted in a Faraday cage	2	5 min
FRM filter samples analyzed by IMPROVE TOR[c]	OC, EC, and TC ($\mu g/m^3$)	Particles collected on a quartz-fiber filter are subjected to different temperature ramps following the IMPROVE TOR protocol. The resulting CO_2 is converted to CH_4 and analyzed by FID. Pyrolysis correction is by laser reflectance.	632.8	$PM_{2.5}$ impactor	Quartz-fiber filter	16.7	24 hr

Notes: [a]MAAP, model 5012, Thermo-Electron, Waltham, MA); 2-AE, model AE-21, Magee Scientific, Berkeley, CA); 7-AE, model AE-31, Magee Scientific, Berkeley, CA); photoacoustic, photoacoustic analyzer (DRI, Reno, NV); Sunset, semicontinuous Sunset Laboratory Carbon Aerosol Analysis Field Instrument (Sunset Laboratory, Tigard, OR) following the National Institute for Occupational Safety and Health (NIOSH) TOT 5040 protocol; R&P 5400, ambient carbon particulate monitor (Rupprecht & Patashnick, Albany, NY); PAS-PAH, particle-bound PAH monitor (model PAS2000, EcoChem Analytics, League City, TX); FRM, Federal Reference Monitor (Andersen Instruments, Smyrna, GA); [b]TSP = total suspended particles; NA = not applicable; PAS = photoelectric aerosol sensor; FID = flame-ionization detector; [c]IMPROVE TOR as in ref. 5.

Fresno Supersite (3425 First Street, Fresno, CA) is located near commercial buildings, restaurants, churches, schools, and residential areas and is ~5.5 km northeast of the downtown Fresno commercial district. First Street is a four-lane artery with moderate traffic levels; sampling inlets are on the rooftop of a two-story building on the

west side of the street. This analysis examines measurements from December 2003 through November 2004.

For the Magee Scientific dual-wavelength (2-AE) and seven-color (7-AE) aethalometers,[31,32] particles are deposited on a quartz-fiber filter tape and the change of light transmission through the filter tape measured by light source and detector is used to calculate 5-min average BC concentrations. The filter tape is automatically advanced when its optical density attains 0.75. The attenuation is converted to a BC mass concentration, using a σ_{abs} of $14625/\lambda$ (m^2/g). In normal operation, corrections are not made for filter loading, filter scattering, or aerosol scattering.[8]

For the Thermo multi-angle absorption photometer (MAAP), samples are deposited on a filter tape similar to the process in the aethalometer.[10,33,34] The MAAP measures reflectance of 670 nm light at 130° and 165° from the projected light beam. Use of these as inputs to a two-stream-approximation radiative transfer model minimizes filter- and aerosol-scattering biases, returning a b_{abs}(670 nm) comparable to that of the photoacoustic analyzer for kerosene smoke and electric arc graphite.[34] An empirical σ_{abs}(670 nm) of 6.5 m^2/g was applied to convert 1-min b_{abs} to BC. Comparison of the MAAP samples with EC derived from the German extraction/thermal desorption method[35] yielded σ_{abs}(670 nm) values of 6.4 ± 1 m^2/g for urban Berlin aerosol, 6.5 ± 0.7 m^2/g for urban Bad Korzingen aerosol, and 4.8 ± 1.2 m^2/g for non-urban Mount Kleiner Feldberg aerosol with EC <0.5 $\mu g/m^3$. The VDI method reports higher fractions of EC than many other methods,[36] including the Interagency Monitoring of Protected Visual Environments (IMPROVE) thermal/optical reflectance (TOR) protocol[17,37,38] applied to $PM_{2.5}$ filter samples at the Fresno Supersite.

The Desert Research Institute (DRI) photoacoustic analyzer measures 5-min average b_{abs}(1047 nm).[20,39,40] An empirical σ_{abs}(1047 nm) of 5 m^2/g was applied to convert photoacoustic b_{abs}(1047 nm) to BC, based on comparison samples from IMPROVE EC and photoacoustic BC measurements of diesel emissions.[40]

The Sunset analyzer,[41,42] which is based on thermal/optical transmittance (TOT), draws air through a quartz-fiber filter for 45 min at 8.5 L/min to obtain the sample. The sampling port is then sealed for 15 min, and the sample is heated to 250, 500, 650, and 850 °C in 100% He, then to 650, 750, 850, and 940 °C in 98% He/2% oxygen (O_2) that backflows through the filter. The evolved carbon is oxidized to carbon dioxide (CO_2), then quantified by a nondispersive IR (NDIR) detector. Charred OC is monitored by transmittance at λ = 660 nm. The carbon that evolves after the transmittance achieves its original value is classified as EC. The filter is presumably free of carbon after the analysis. The sampling inlet is opened, and the cycle begins again for the next hour. This unit also monitors the transmitted laser signal during the collection phase to obtain a BC measurement by the same principle as applied in the aethalometer.

For the R&P 5400 carbon monitor,[43] particles are drawn through a $PM_{2.5}$ inlet, deposited on an impactor, and heated by a Xenon lamp to 275 °C in air, combusted to CO_2, and measured with an NDIR to determine 1-hr average OC. The temperature is increased to 750 °C to measure total carbon (TC). EC is determined based on the difference between TC and OC.

The EcoChem particle-bound polycyclic aromatic hydrocarbon (PAH) monitor[44] uses a photoelectric sensor with an excimer lamp that produces UV radiation (225 nm) to photo-ionize the sampled particles. This photon energy minimizes ionization of gas molecules. The charged particles are collected on a filter element mounted in a Faraday cage, and the electric current is measured with an electrometer. The photoelectric current is proportional to the concentration of particle-bound PAHs, weighted according to an average ionization response. This is a relative measure of particle-bound PAH; therefore, the results are reported in terms of the electrometer output in femptoamps (fA).

These continuous BC measurements are compared with each other and with EC determined by IMPROVE-TOR analysis[17,37,38] of 24-hr quartz-fiber filters from a $PM_{2.5}$ Federal Reference Monitor (FRM)[45] operated every sixth day. Filters were baked at 900 °C for 4 hr before sampling to remove adsorbed organic vapors.[46] For IMPROVE_TOR analysis, the sample is heated in successive steps of 120 °C (OC1), 250 °C (OC2), 450 °C (OC3), and 550 °C (OC4) in He and 550 °C (EC1), 700 °C (EC2), and 800 °C (EC3) in 98% He/2% O_2. Evolved carbon is oxidized to CO_2 and then reduced to methane (CH_4) for detection by a flame-ionization detector (FID). The pyrolyzed (i.e., charred) OC is monitored by reflectance at λ = 632.8 nm. Until the laser signal returns to its initial value, the portion of EC1 is assigned to pyrolyzed OC (OP). The OC is defined by the sum of OC1, OC2, OC3, OC4, and OP, whereas the EC is defined by EC1 + EC2 + EC3 − OP.

Other continuous measurements examined in this analysis include (1) ultrafine and fine particle numbers from nano (3–84 nm) and standard (84–407 nm) scanning mobility particle sizers (SMPS; models 3936N25A and 3936L10, TSI, Shoreview, MN); [5,47] (2) b_{scat}(530 nm) by nephelometer (Radiance Research M903, Seattle, WA);[48] (3) $PM_{2.5}$ mass concentration by tapered element oscillating microbalance (TEOM; model 1400a, Rupprecht and Patashnick, Albany, NY);[49] (4) NO_3^- by flash volatilization (model R&P 8400N, Rupprecht and Patashnick, Albany, NY);[50] (5) NO_x by chemiluminescence (model TEI 42, Thermo Electron Inc., Franklin, MA); (6) CO by IR gas filter correlation (model DASIBI 3008, Environmental Corp., Glendale, CA); (7) O_3 by UV absorption (model API 400, API Inc., San Diego, CA); and (8) meteorology measurements (i.e., wind speed and direction [model 05305L high-sensitivity wind vane and anemometer, Met One, Grants Pass, OR], temperature [model CS500L platinum resistance sensor, Met One], relative humidity [RH; model CS capacitance sensor, Met One], solar radiation [model LI200X-L pyranometer, Li-Cor, Lincoln, NE], and atmospheric pressure [model Met One piezofilm sensor, Met One]).

RESULTS

Comparison of BC and EC Measurements

Table 2 lists comparability statistics, obtained with the assumed $\sigma_{abs}(\lambda)$, for the different BC and EC measurements. These statistics reflect the differences evident in

Table 2. Comparison statistics for collocated BC and EC measurements between December 1, 2003, and November 30, 2004

Sampling period	Methods[a] y	Methods[a] x	No. of Pairs	Average of Ratios (y/x ± SD)	Distribution of Differences[b] (%) <1σ[c]	1σ–2σ	2σ–3σ	>3σ	Average Difference of y − x (μg/m³)	Correlation (r)	Regression Slope ± Standard Error	Intercept ± Standard Error (μg/m³)
	DRI/OGC	Photoacoustic at 1047 nm										
Dec 2003–Feb 2004	IMPROVE EC		14	2.24 ± 0.40	0	0	7	93	1.28	0.97	2.09 ± 0.14	0.09 ± 0.18
June 2004–Aug 2004	IMPROVE EC		16	1.82 ± 0.24	13	38	38	13	0.33	0.99	1.59 ± 0.07	0.07 ± 0.03
	MAAP at 670 nm	Photoacoustic at 1047 nm										
Dec 2003			491	1.99 ± 0.80	17	26	12	45	1.19	0.99	1.78 ± 0.01	0.14 ± 0.02
Jan 2004			696	1.83 ± 0.27	6	26	24	44	0.88	0.99	1.81 ± 0.01	0.00 ± 0.02
Feb 2004			672	1.83 ± 0.39	19	26	13	42	0.67	0.99	1.80 ± 0.01	0.00 ± 0.01
Mar 2004			719	1.80 ± 0.39	11	18	21	50	0.46	0.98	1.68 ± 0.01	0.04 ± 0.01
Apr 2004			673	1.75 ± 0.54	17	26	18	39	0.25	0.97	1.55 ± 0.02	0.04 ± 0.01
May 2004			730	1.70 ± 0.54	18	25	18	39	0.17	0.96	1.49 ± 0.02	0.03 ± 0.01
Jun 2004			714	1.71 ± 0.43	11	22	23	44	0.19	0.97	1.52 ± 0.02	0.03 ± 0.01
Jul 2004			743	1.67 ± 0.37	9	21	29	41	0.25	0.96	1.44 ± 0.02	0.07 ± 0.01
Aug 2004			168	1.63 ± 0.43	12	35	15	32	0.20	0.95	1.45 ± 0.04	0.04 ± 0.02
	7-AE at 880 nm	Photoacoustic at 1047 nm										
Dec 2003			514	1.45 ± 0.62	27	21	13	33	0.50	0.99	1.33 ± 0.01	0.06 ± 0.01
Jan 2004			697	1.42 ± 0.22	19	30	17	33	0.42	0.98	1.35 ± 0.01	0.04 ± 0.01
Feb 2004			672	1.96 ± 0.71	17	18	11	53	0.77	0.96	1.89 ± 0.02	0.05 ± 0.03
Mar 2004			720	1.61 ± 0.33	15	18	18	48	0.35	0.97	1.50 ± 0.01	0.05 ± 0.01
Apr 2004			695	1.54 ± 0.47	21	22	19	37	0.18	0.96	1.38 ± 0.02	0.03 ± 0.01
May 2004			714	1.61 ± 0.51	18	20	19	43	0.15	0.96	1.42 ± 0.01	0.03 ± 0.01
Jun 2004			695	1.67 ± 0.58	12	21	18	49	0.17	0.95	1.56 ± 0.02	0.01 ± 0.01
Jul 2004			743	1.58 ± 0.36	14	24	23	39	0.22	0.95	1.40 ± 0.02	0.05 ± 0.01
Aug 2004			743	1.46 ± 0.37	25	31	16	28	0.23	0.96	1.37 ± 0.02	0.02 ± 0.01
	Sunset optical at 660 nm	Photoacoustic at 1047 nm										
Dec 2003			297	0.91 ± 0.19	79	19	1	0	−0.15	0.99	0.92 ± 0.01	−0.04 ± 0.01
Jan 2004			717	0.82 ± 0.13	59	25	11	5	−0.19	0.98	0.86 ± 0.01	−0.04 ± 0.01
Feb 2004			540	0.79 ± 0.17	48	28	8	14	−0.19	0.99	0.78 ± 0.01	0.00 ± 0.01
Mar 2004			394	0.89 ± 0.22	60	27	4	6	−0.10	0.98	0.79 ± 0.01	0.03 ± 0.01
Apr 2004			682	0.89 ± 0.27	55	27	11	7	−0.06	0.97	0.82 ± 0.01	0.01 ± 0.00
May 2004			712	0.94 ± 0.35	55	28	9	8	−0.04	0.90	0.78 ± 0.01	0.03 ± 0.01
Jun 2004			694	0.92 ± 0.32	57	31	7	4	−0.04	0.96	0.89 ± 0.01	−0.01 ± 0.00
Jul 2004			717	0.98 ± 0.31	69	20	4	7	−0.02	0.85	0.90 ± 0.02	0.02 ± 0.01
Aug 2004			441	1.00 ± 0.32	66	26	4	3	−0.02	0.95	0.95 ± 0.01	0.01 ± 0.01
	Sunset thermal	Photoacoustic at 1047 nm										
Dec 2003			287	1.18 ± 0.42	72	19	3	2	0.18	0.97	1.09 ± 0.02	0.05 ± 0.03
Jan 2004			691	1.21 ± 0.39	62	28	7	3	0.16	0.95	1.08 ± 0.01	0.07 ± 0.02
Feb 2004			448	1.27 ± 0.37	59	27	5	5	0.21	0.96	1.10 ± 0.01	0.11 ± 0.02
Mar 2004			373	1.28 ± 0.56	52	34	6	2	0.12	0.93	1.02 ± 0.02	0.11 ± 0.02
Apr 2004			319	1.05 ± 0.35	54	33	4	3	0.00	0.89	0.82 ± 0.02	0.11 ± 0.02
May 2004			307	1.34 ± 0.79	43	24	6	19	0.06	0.77	0.82 ± 0.04	0.12 ± 0.02
Jun 2004			396	1.00 ± 0.51	41	27	9	15	0.00	0.87	0.94 ± 0.03	0.02 ± 0.01
Jul 2004			579	1.22 ± 0.71	35	29	13	19	0.05	0.62	0.71 ± 0.04	0.18 ± 0.02
Aug 2004			286	1.08 ± 0.35	59	29	4	2	0.02	0.91	0.88 ± 0.02	0.11 ± 0.02
	R&P thermal	Photoacoustic at 1047 nm										
Dec 2003			322	0.57 ± 0.64	17	16	4	57	−0.96	0.81	0.22 ± 0.01	0.21 ± 0.02
Jan 2004			697	0.77 ± 0.84	25	20	13	42	−0.49	0.24	0.15 ± 0.02	0.44 ± 0.03
Feb 2004			665	0.96 ± 1.46	28	21	10	41	−0.37	0.25	0.18 ± 0.03	0.31 ± 0.03
Mar 2004			703	0.81 ± 0.86	28	19	17	36	−0.17	0.13	0.40 ± 0.11	0.27 ± 0.08
Apr 2004			671	0.95 ± 0.62	39	26	12	22	−0.13	0.69	0.26 ± 0.01	0.16 ± 0.01
May 2004			707	1.13 ± 0.72	43	29	12	15	−0.04	0.43	0.29 ± 0.02	0.16 ± 0.01
Jun 2004			367	1.07 ± 0.81	36	30	8	19	−0.07	0.43	0.31 ± 0.03	0.14 ± 0.01

Table 2. Cont.

Sampling period	Methods[a] y	Methods[a] x	No. of Pairs	Average of Ratios (y/x ± SD)	Distribution of Differences[b] (%) <1σ[c]	1σ–2σ	2σ–3σ	>3σ	Average Difference of y − x (μg/m³)	Correlation (r)	Regression Slope ± Standard Error	Intercept ± Standard Error (μg/m³)
	PAH	Photoacoustic at 1047 nm										
Dec 2003			323	NA NA	NA	NA	NA	NA	NA	0.91	11.42 ± 0.29	1.34 ± 0.51
Jan 2004			NA	NA NA	NA	NA	NA	NA	NA	NA	NA ± NA	NA ± NA
Feb 2004			632	NA NA	NA	NA	NA	NA	NA	0.95	9.49 ± 0.13	−0.78 ± 0.14
Mar 2004			720	NA NA	NA	NA	NA	NA	NA	0.81	8.64 ± 0.24	−1.36 ± 0.17
Apr 2004			683	NA NA	NA	NA	NA	NA	NA	0.76	5.25 ± 0.17	−0.07 ± 0.08
May 2004			706	NA NA	NA	NA	NA	NA	NA	0.77	4.54 ± 0.14	0.22 ± 0.05
Jun 2004			695	NA NA	NA	NA	NA	NA	NA	0.78	3.52 ± 0.11	0.30 ± 0.04
Jul 2004			720	NA NA	NA	NA	NA	NA	NA	0.70	4.06 ± 0.16	−0.07 ± 0.08
Aug 2004			720	NA NA	NA	NA	NA	NA	NA	0.73	4.56 ± 0.16	−0.41 ± 0.11
	2-AE at 880 nm	7-AE at 880 nm										
Dec 2003			719	1.07 ± 0.12	87	9	3	1	0.07	0.99	0.99 ± 0.00	0.09 ± 0.01
Jan 2004			750	1.03 ± 0.11	89	9	2	1	0.03	0.99	0.99 ± 0.01	0.03 ± 0.01
Feb 2004			672	1.04 ± 0.11	89	8	3	1	0.01	0.99	0.96 ± 0.00	0.05 ± 0.01
Mar 2004			720	1.04 ± 0.09	94	5	1	0	0.02	0.99	0.99 ± 0.01	0.03 ± 0.01
Apr 2004			527	1.04 ± 0.21	88	8	2	1	0.01	0.98	1.01 ± 0.01	0.01 ± 0.01
May 2004			252	1.09 ± 0.11	83	13	1	2	0.03	0.99	1.09 ± 0.01	0.00 ± 0.00
Jun 2004			696	1.07 ± 0.10	86	10	3	1	0.03	0.98	1.00 ± 0.01	0.03 ± 0.00
Jul 2004			744	1.09 ± 0.11	81	15	2	1	0.05	0.98	1.05 ± 0.01	0.02 ± 0.01
Aug 2004			744	1.09 ± 0.10	84	11	3	2	0.07	0.99	1.08 ± 0.01	0.01 ± 0.01
Sep 2004			702	1.07 ± 0.12	82	14	3	1	0.05	0.98	1.01 ± 0.01	0.04 ± 0.01
Oct 2004			629	1.14 ± 0.19	73	18	7	2	0.13	0.99	1.03 ± 0.01	0.09 ± 0.01
Nov 2004			660	1.12 ± 0.13	77	16	4	3	0.20	0.99	1.08 ± 0.01	0.05 ± 0.01
	2-AE at 370 nm	7-AE at 370 nm										
Dec 2003			719	1.16 ± 0.26	71	18	6	4	0.22	0.99	1.06 ± 0.01	0.09 ± 0.02
Jan 2004			750	1.10 ± 0.22	71	20	6	3	0.12	0.98	1.02 ± 0.01	0.08 ± 0.02
Feb 2004			672	1.10 ± 0.24	75	18	4	2	0.07	0.99	0.99 ± 0.01	0.08 ± 0.01
Mar 2004			720	1.07 ± 0.16	68	24	5	3	0.05	0.97	1.01 ± 0.01	0.05 ± 0.01
Apr 2004			527	1.07 ± 0.18	72	18	5	3	0.02	0.96	1.02 ± 0.01	0.01 ± 0.01
May 2004			252	1.14 ± 0.16	69	23	2	4	0.04	0.98	1.08 ± 0.01	0.01 ± 0.01
Jun 2004			696	1.12 ± 0.15	67	23	6	4	0.04	0.97	1.00 ± 0.01	0.04 ± 0.01
Jul 2004			744	1.13 ± 0.16	62	26	8	4	0.07	0.96	1.05 ± 0.01	0.04 ± 0.01
Aug 2004			744	1.14 ± 0.15	.67	20	8	6	0.09	0.97	1.10 ± 0.01	0.02 ± 0.01
Sep 2004			702	1.12 ± 0.17	64	22	9	5	0.08	0.97	1.02 ± 0.01	0.06 ± 0.01
Oct 2004			629	1.18 ± 0.23	62	22	10	6	0.16	0.98	1.05 ± 0.01	0.10 ± 0.01
Nov 2004			660	1.17 ± 0.20	64	22	8	5	0.29	0.99	1.11 ± 0.01	0.06 ± 0.02
	PAH	7-AE at 370 nm										
Dec 2003			543	NA NA	NA	NA	NA	NA	NA	0.91	7.03 ± 0.14	−0.41 ± 0.40
Jan 2004			NA	NA NA	NA	NA	NA	NA	NA	NA	NA ± NA	NA ± NA
Feb 2004			632	NA NA	NA	NA	NA	NA	NA	0.92	4.70 ± 0.08	−0.40 ± 0.17
Mar 2004			720	NA NA	NA	NA	NA	NA	NA	0.84	5.62 ± 0.13	−1.44 ± 0.15
Apr 2004			696	NA NA	NA	NA	NA	NA	NA	0.74	3.71 ± 0.13	−0.16 ± 0.09
May 2004			719	NA NA	NA	NA	NA	NA	NA	0.71	2.80 ± 0.11	0.33 ± 0.06
Jun 2004			696	NA NA	NA	NA	NA	NA	NA	0.79	2.50 ± 0.07	0.25 ± 0.04
Jul 2004			719	NA NA	NA	NA	NA	NA	NA	0.73	3.17 ± 0.11	−0.24 ± 0.07
Aug 2004			719	NA NA	NA	NA	NA	NA	NA	0.71	3.59 ± 0.13	−0.45 ± 0.12
	DRI/OGC	MAAP at 670 nm										
Dec 2003–Feb 2004	IMPROVE EC	MAAP	13	1.18 ± 0.18	31	23	23	23	0.98	0.33	1.16 ± 0.07	0.01 ± 0.16
June 2004–Aug 2004	IMPROVE EC	MAAP	12	1.12 ± 0.13	67	25	8	0	0.98	0.05	0.94 ± 0.06	0.09 ± 0.03
	DRI/OGC	7-AE at 880 nm										
Dec 2003–Feb 2004	IMPROVE EC	7-AE	15	1.64 ± 0.32	7	7	33	53	0.95	0.88	1.49 ± 0.14	0.13 ± 0.24
June 2004–Aug 2004	IMPROVE EC	7-AE	16	1.23 ± 0.2	69	25	6	0	0.97	0.12	1.08 ± 0.07	0.06 ± 0.05
	Photoacoustic at 1047 nm	MAAP at 670 nm										
Dec 2003			491	0.53 ± 0.09	17	26	12	45	0.99	−1.19	0.55 ± 0.00	−0.05 ± 0.01
Jan 2004			696	0.56 ± 0.08	6	26	24	44	0.99	−0.88	0.54 ± 0.00	0.03 ± 0.01

Table 2. Cont.

Sampling period	Methods[a] y	Methods[a] x	No. of Pairs	Average of Ratios ($y/x \pm$ SD)	Distribution of Differences[b] (%) <1σ[c]	1σ–2σ	2σ–3σ	>3σ	Average Difference of $y - x$ (μg/m³)	Correlation (r)	Regression Slope ± Standard Error	Intercept ± Standard Error (μg/m³)
Feb 2004			672	0.57 ± 0.17	19	26	13	42	0.99	−0.67	0.54 ± 0.00	0.01 ± 0.01
Mar 2004			719	0.57 ± 0.10	11	18	21	50	0.98	−0.46	0.57 ± 0.00	0.00 ± 0.00
Apr 2004			673	0.62 ± 0.17	17	26	18	39	0.97	−0.25	0.60 ± 0.01	0.01 ± 0.01
May 2004			730	0.64 ± 0.17	18	25	18	39	0.96	−0.17	0.62 ± 0.01	0.00 ± 0.00
Jun 2004			714	0.62 ± 0.15	11	22	23	44	0.97	−0.19	0.61 ± 0.01	0.00 ± 0.00
Jul 2004			743	0.62 ± 0.12	9	21	29	41	0.96	−0.25	0.64 ± 0.01	−0.01 ± 0.01
Aug 2004			168	0.65 ± 0.15	12	35	15	32	0.95	−0.20	0.63 ± 0.02	0.01 ± 0.01
	7-AE at 880 nm	MAAP at 670 nm										
Dec 2003			645	0.75 ± 0.08	46	24	11	19	0.99	−0.63	0.72 ± 0.00	0.04 ± 0.01
Jan 2004			720	0.77 ± 0.08	42	32	14	13	0.99	−0.44	0.74 ± 0.00	0.05 ± 0.01
Feb 2004			672	0.82 ± 0.10	55	21	9	15	0.99	−0.31	0.77 ± 0.00	0.04 ± 0.01
Mar 2004			720	0.90 ± 0.09	80	13	3	4	0.98	−0.10	0.88 ± 0.01	0.03 ± 0.01
Apr 2004			696	0.89 ± 0.10	71	23	3	3	0.99	−0.07	0.88 ± 0.00	0.00 ± 0.00
May 2004			720	0.96 ± 0.14	85	10	3	2	0.98	−0.02	0.91 ± 0.01	0.02 ± 0.00
Jun 2004			695	0.96 ± 0.12	87	11	1	1	0.98	0.02	1.02 ± 0.01	−0.03 ± 0.00
Jul 2004			743	0.95 ± 0.14	83	14	3	1	0.97	−0.03	0.95 ± 0.01	0.00 ± 0.01
Aug 2004			168	0.92 ± 0.08	84	10	4	3	0.99	−0.05	0.86 ± 0.01	0.02 ± 0.01
	7-AE at 660 nm	MAAP at 670 nm										
Dec 2003			645	0.79 ± 0.08	52	23	10	15	0.99	−0.53	0.76 ± 0.00	0.04 ± 0.01
Jan 2004			720	0.81 ± 0.08	51	31	12	7	0.99	−0.36	0.80 ± 0.00	0.02 ± 0.01
Feb 2004			672	0.89 ± 0.11	69	19	6	6	0.99	−0.20	0.85 ± 0.00	0.03 ± 0.01
Mar 2004			720	0.94 ± 0.09	92	6	1	0	0.98	−0.06	0.92 ± 0.01	0.02 ± 0.01
Apr 2004			696	0.94 ± 0.11	83	13	3	1	0.99	−0.04	0.92 ± 0.01	0.01 ± 0.00
May 2004			720	1.00 ± 0.13	86	9	3	2	0.98	0.00	0.93 ± 0.01	0.03 ± 0.00
Jun 2004			695	1.01 ± 0.11	90	8	1	1	0.98	0.01	1.05 ± 0.01	−0.02 ± 0.00
Jul 2004			743	1.00 ± 0.16	86	11	2	1	0.97	0.00	0.99 ± 0.01	0.01 ± 0.01
Aug 2004			168	0.97 ± 0.08	90	6	4	0	0.99	−0.02	0.92 ± 0.01	0.02 ± 0.01
	Sunset optical at 660 nm	MAAP at 670 nm										
Dec 2003			559	0.45 ± 0.05	14	27	17	42	0.99	−1.40	0.49 ± 0.00	−0.06 ± 0.01
Jan 2004			717	0.44 ± 0.05	3	24	26	46	0.99	−1.09	0.48 ± 0.00	−0.04 ± 0.01
Feb 2004			452	0.42 ± 0.05	2	29	21	48	0.99	−1.11	0.43 ± 0.00	−0.01 ± 0.01
Mar 2004			397	0.48 ± 0.06	6	22	25	48	0.98	−0.62	0.47 ± 0.01	0.01 ± 0.02
Apr 2004			361	0.51 ± 0.07	6	23	27	44	0.96	−0.45	0.53 ± 0.01	−0.02 ± 0.01
May 2004			711	0.55 ± 0.07	8	37	22	33	0.97	−0.28	0.57 ± 0.01	−0.01 ± 0.01
Jun 2004			694	0.51 ± 0.07	1	19	43	38	0.98	−0.31	0.61 ± 0.01	−0.05 ± 0.00
Jul 2004			716	0.59 ± 0.10	5	42	32	21	0.95	−0.26	0.69 ± 0.01	−0.05 ± 0.01
Aug 2004			167	0.75 ± 0.17	51	28	12	9	0.90	−0.15	0.72 ± 0.03	0.01 ± 0.02
	Sunset thermal	MAAP at 670 nm										
Dec 2003			559	0.63 ± 0.20	33	22	16	28	0.98	−1.05	0.59 ± 0.01	0.03 ± 0.02
Jan 2004			691	0.65 ± 0.17	27	32	16	25	0.96	−0.74	0.60 ± 0.01	0.05 ± 0.02
Feb 2004			448	0.67 ± 0.19	32	29	19	20	0.98	−0.67	0.61 ± 0.01	0.08 ± 0.02
Mar 2004			373	0.69 ± 0.22	31	29	19	21	0.94	−0.40	0.61 ± 0.01	0.01 ± 0.01
Apr 2004			319	0.58 ± 0.25	17	31	20	32	0.88	−0.38	0.56 ± 0.02	0.03 ± 0.02
May 2004			331	0.68 ± 0.39	26	36	16	22	0.88	−0.19	0.89 ± 0.03	−0.12 ± 0.02
Jun 2004			369	0.63 ± 0.26	20	27	25	28	0.88	−0.25	0.59 ± 0.02	0.02 ± 0.01
Jul 2004			572	0.73 ± 0.39	30	30	19	21	0.70	−0.23	0.54 ± 0.02	0.11 ± 0.02
Aug 2004			94	0.73 ± 0.37	33	27	22	18	0.77	−0.20	0.58 ± 0.05	0.09 ± 0.04

Notes: [a]7-AE (in μg/m³) at 370, 660, or 880 nm, 7-AE BC (in μg/m³) at $\lambda = 370$, 660, 880 nm, respectively; MAAP BC (in μg/m³), at $\lambda = 670$ nm; R&P thermal, EC (in μg/m³) thermally determined by R&P 5400 ambient carbon particulate monitor; IMPROVE EC (in μg/m³), measured by the DRI/OGC TOR carbon analyzer following the IMPROVE protocol; Sunset optical, EC (in μg/m³) optically determined ($\lambda = 660$ nm) with the Sunset Laboratory carbon analyzer; Sunset thermal, EC (in μg/m³) determined by Sunset Laboratory carbon analyzer following the NIOSH 5040 protocol; PAH, particle-bound PAHs (in fA) measured by photoelectric aerosol sensor monitor; [b]Fraction of pairs in percent with which the difference ($y - x$) is less than or greater than one, two, or three times propagated measurement uncertainty (note that the precision interval, σ, is different from the mass absorption efficiency, σ_{abs}); [c]Measurement uncertainty of ($y - x$).

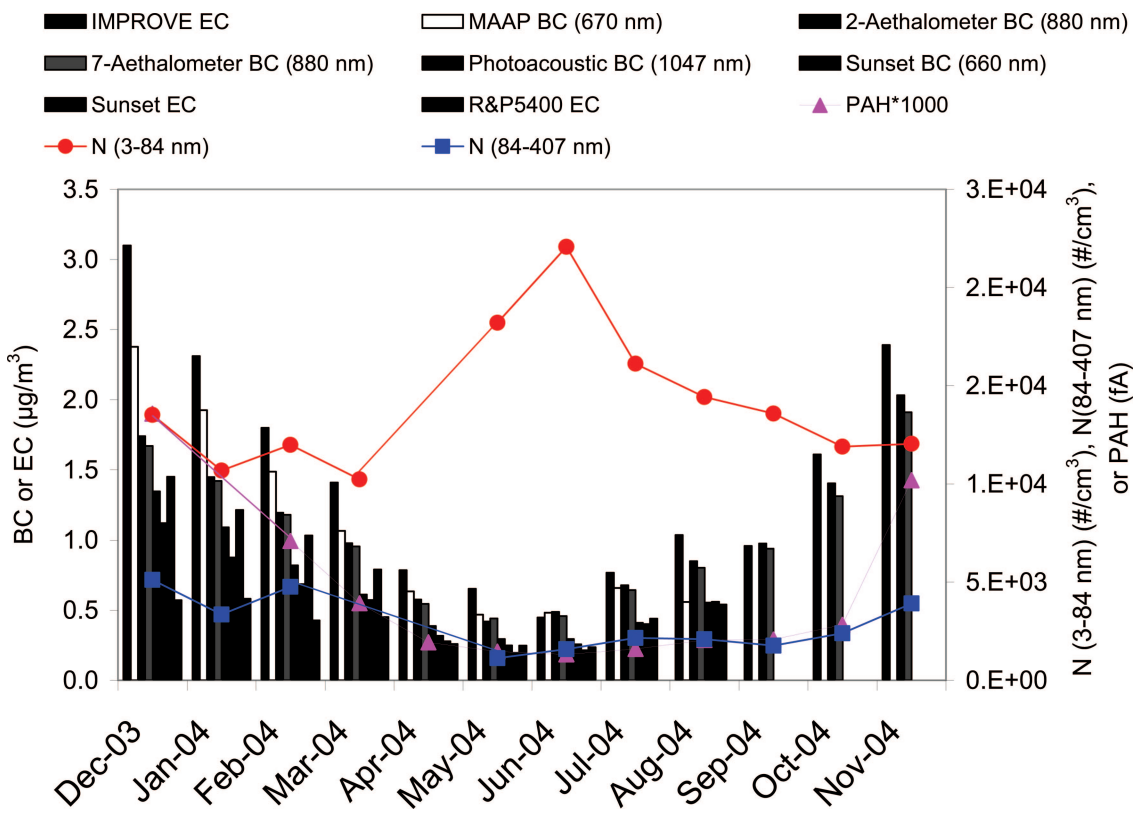

Figure 1. Monthly averages of BC or EC concentrations measured by eight carbon methods, particle-bound PAH, and particle number concentrations in two size ranges (3–84 nm and 84–407 nm) for ambient samples at the Fresno Supersite from December 2003 to November 2004.

Figure 1. The average of y/x with its standard deviation, the distribution of the difference $(y - x)$ between data pairs where σ is the measurement uncertainty (i.e., the square root of the sum of squared uncertainties), the average of the differences $(\overline{y - x})$, the linear correlation coefficient (r), and the regression slopes and intercepts with standard errors are calculated for each comparison.[28]

Data-pair requirements for carbon equivalence are met when the regression slope is 1 ± 0.05, the regression intercept is 0 ± 1 μg/m^3 ($r > 0.97$), and the collocated precision is 2 μg/m^3 or 5% (whichever is larger).[28] Comparability is attained when the regression slope equals unity within three standard errors, the regression intercept does not differ from zero by more than three standard errors, and r is >0.9. Predictability is attained when r is >0.9, but the slope and intercept exceeded those required for comparability. The equivalence criteria were established for $PM_{2.5}$ mass comparison by the U.S. Environmental Protection Agency and are too stringent for the comparison of $PM_{2.5}$ components.

As shown in Table 2, the average difference $(\overline{y - x})$ was typically <0.5 μg/m^3 with a few exceptions, and in no case did the $\overline{y - x}$ exceed 1.4 μg/m^3 of BC. The collocated 7-AE BC and 2-AE BC results met the equivalence criteria except during the months of May, August, and November 2004, when slopes were within ~10% of unity; hereafter, the 7-AE BC results are used to represent aethalometer BC. The filter-based IMPROVE EC results are highly correlated with the photoacoustic BC results ($0.97 < r < 0.99$), but the IMPROVE EC slope indicates a 1.5 to 2 times higher concentration than the photoacoustic analyzer, using the $\sigma_{abs}(1047) = 5$ m^2/g conversion. Compared with the photoacoustic BC results, the MAAP BC, 7-AE BC, Sunset optical (BC), Sunset thermal EC, and PAH values in winter also show high correlations ($r > 0.9$), but the slopes and average ratios differ from unity. The intercepts for these comparisons are well within 1 μg/m^3, but the slopes vary from unity within a factor of 2. Photoacoustic BC was much lower than either aethalometer or MAAP BC, as evidenced by the high slopes (1.3–2).

Sunset thermal EC results correlate better with the photoacoustic BC results in winter (December 2003 to February 2004; $0.95 < r < 0.97$) than in summer (June to August 2004; $0.62 < r < 0.91$), with slopes indicating a Sunset EC ~10% higher than the photoacoustic BC in winter and 5–30% lower than photoacoustic BC in summer. Compared with photoacoustic BC, the distribution of differences shows that ~80% of the Sunset thermal and ~85% of Sunset optical BC values are within ±3 precision intervals. Particle-bound PAH levels show higher correlations with photoacoustic BC for winter ($0.91 < r < 0.95$) than for summer ($0.70 < r < 0.78$). The R&P 5400 EC is not well correlated with the photoacoustic BC except for December 2003 ($r = 0.81$).

When the MAAP ($\lambda = 670$ nm) BC or 7-AE value is used as the benchmark, IMPROVE EC meets the requirements for comparability. The IMPROVE EC versus MAAP BC comparison almost meets the equivalence criteria in summer except for a lower slope (0.94 ± 0.06). The MAAP

Table 3. Comparisons of carbon measurement methods with overall averages of BC or EC for collocated periods between December 1, 2003, and November 30, 2004, at the Fresno Supersite.

Sampling Period	Methods y^b	Methods x	No. of Pairs	Average of Ratios $y/x \pm$ SD	Distribution of Differences (%) $<1\sigma^a$	1σ–2σ	2σ–3σ	$>3\sigma$	Correlation (r)	Average Difference of $y - x$	Regression Slope ± Standard Error	Intercept ± Standard Error
	IMPROVE EC	All methods average										
Winter			15	1.58 ± 0.22	20	67	7	7	0.98	0.85	1.50 ± 0.08	0.07 ± 0.15
Summer			15	1.38 ± 0.14	67	33	0	0	0.99	0.18	1.19 ± 0.03	0.08 ± 0.02
Dec 2003–Aug 2004			45	1.45 ± 0.21	62	20	13	4	0.98	0.42	1.53 ± 0.04	−0.07 ± 0.05
	7-AE at 880 nm	All methods average										
Winter			15	0.98 ± 0.09	100	0	0	0	0.99	−0.03	0.96 ± 0.04	0.03 ± 0.08
Summer			15	1.14 ± 0.01	93	7	0	0	0.99	0.08	1.15 ± 0.05	0.00 ± 0.03
Dec 2003–Aug 2004			45	1.08 ± 0.12	100	0	0	0	0.99	0.04	0.96 ± 0.02	0.08 ± 0.03
	Photoacoustic at 1047 nm	All methods average										
Winter			15	0.72 ± 0.06	71	21	7	0	0.99	−0.41	0.72 ± 0.02	0.01 ± 0.04
Summer			15	0.76 ± 0.06	87	13	0	0	0.99	−0.13	0.78 ± 0.02	−0.01 ± 0.02
Dec 2003–Aug 2004			44	0.74 ± 0.07	73	23	2	2	0.99	−0.24	0.72 ± 0.02	0.01 ± 0.02
	Sunset optical at 660 nm	All methods average										
Winter			14	0.57 ± 0.06	21	71	7	0	0.99	−0.66	0.69 ± 0.02	−0.16 ± 0.03
Summer			14	0.73 ± 0.12	86	14	0	0	0.98	−0.13	0.96 ± 0.06	−0.11 ± 0.04
Dec 2003–Aug 2004			41	0.66 ± 0.14	73	12	15	0	0.98	−0.34	0.64 ± 0.02	0.01 ± 0.03
	Sunset thermal	All methods average										
Winter			14	0.81 ± 0.08	86	14	0	0	0.99	−0.30	0.76 ± 0.03	0.08 ± 0.06
Summer			12	0.75 ± 0.18	92	8	0	0	0.98	−0.12	0.98 ± 0.06	−0.11 ± 0.04
Dec 2003–Aug 2004			35	0.78 ± 0.18	96	4	0	0	0.98	−0.21	0.81 ± 0.03	−0.01 ± 0.04
	MAAP at 670 nm	All methods average										
Winter			14	1.30 ± 0.07	57	36	7	0	1.00	0.50	1.35 ± 0.02	−0.05 ± 0.04
Summer			12	1.21 ± 0.06	100	0	0	0	1.00	0.10	1.27 ± 0.03	−0.02 ± 0.01
Dec 2003–Aug 2004			41	1.24 ± 0.10	71	15	12	2	1.00	0.26	1.34 ± 0.02	−0.05 ± 0.02

Notes: [a]The precision interval, σ, is different from the mass absorption efficiency, σ_{abs}; [b]See Table 2 for different measurement method specifications.

BC values are typically 30–50% higher than the photoacoustic and Sunset BC values, with small intercepts (<0.1 ± 0.02 $\mu g/m^3$). The best comparison is found for 7-AE values at λ = 660 or 880 nm and MAAP BC values, for which >70% of the samples are within ±2 precision intervals and >80% of the samples are within ±3 precision intervals.

Table 3 compares values from each instrument with the overall averages of all measurements, weighted by the number of available data points. BC or EC values from each method correlate well with the average ($r \geq 0.98$), but regression slopes range from 0.64 (Sunset optical BC) to 1.53 (IMPROVE EC). For the overall averages, Sunset optical BC and Sunset thermal EC meet the comparability criteria during summer, whereas 7-AE BC meets the criteria in both winter and summer seasons. Deviations from unity are 10–20% higher for winter (from −31% [Sunset optical] to +50% [IMPROVE EC]) than for summer (from −22% [photoacoustic] to +27% [MAAP]). The distribution of differences shows that >85% of the samples are within ±2 precision intervals and >90% of the samples are within ±3 precision intervals. All of the samples are within ±1 precision interval for the aethalometer in both the winter and annual periods and for the MAAP in summer.

Seasonal Variation

As shown in Figure 1, monthly averaged BC or EC concentrations were ~2.2 to 3.4 times higher during winter than summer. This is because of higher BC or EC contributions from traffic emissions in cold conditions, heating (including RWC), and accumulation of pollutants in a shallow surface layer during non-daylight hours. $PM_{2.5}$ BC and EC concentrations among different methods differed by as much as a factor of 5 during the winter, with IMPROVE EC being the highest and R&P 5400 EC being the lowest. Despite their similarities, the three thermal methods (IMPROVE, Sunset, and R&P 5400) yielded monthly EC concentrations ranging from 0.2 $\mu g/m^3$ (Sunset) to 3.1 $\mu g/m^3$ (IMPROVE), with 3-fold higher EC concentrations in winter (1.39 ug/m^3) than in summer (0.46 $\mu g/m^3$). Different temperature- and charring-correction protocols give different values of EC at Fresno.[17,29]

The three optical methods (MAAP, 7-AE, and Sunset optical) yielded monthly BC concentrations from 0.25 $\mu g/m^3$ (Sunset) to 2.38 $\mu g/m^3$ (15.5 Mm^{-1}; MAAP), also approximately three times higher in winter (1.42 ug/m^3) than in summer (0.54 $\mu g/m^3$). The monthly averaged PAH concentration was consistent with the variation of BC or EC concentrations, with PAH concentrations six times higher in winter than summer.

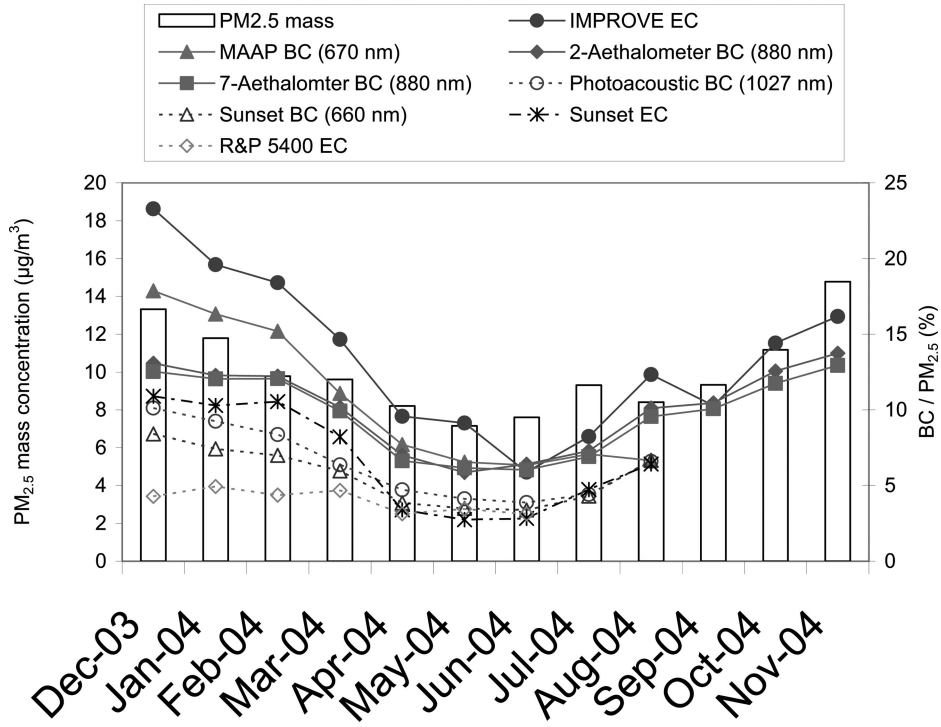

Figure 2. Monthly averages of $PM_{2.5}$ by TEOM and the ratio of BC or EC to $PM_{2.5}$ by IMPROVE, by MAAP (λ = 670 nm), by 2-AE (λ = 880 nm), by 7-AE (λ = 880 nm), by photoacoustic instrument (λ = 1047 nm), by Sunset optical (λ = 660 nm), by Sunset thermal, or by R&P 5400.

Ultrafine particle-number concentrations in the 3–84 nm size range [N(3–84 nm)] were higher during the summer, whereas the accumulation mode particle-number concentrations in the 84–407 nm range followed the BC or EC seasonal pattern. Watson et al.[47,51] observed frequent secondary ultrafine particle events during late spring through early fall. BC or EC are derived from primary emissions that accumulate during the winter when dispersion is low.[50]

Figure 2 shows how BC and EC concentrations varied with $PM_{2.5}$ throughout the year. The ratio of BC or EC to $PM_{2.5}$ ranged from 7% to 23% during winter and from 3% to 12% during summer (exclusive of the R&P 5400). Figure 3 shows how OC/EC ratios varied throughout the year. $PM_{2.5}$ OC/EC ratios were >78% higher during the summer (5.7) than during winter (3.2). This may result from (1) many EC concentrations during summer that were near the lower quantifiable limits, resulting in higher uncertainty in the denominator (EC concentrations were <1 $\mu g/m^3$ for ~75% of the days during summer); (2) higher contributions from secondary organic aerosol (SOA) during summer; (3) larger contributions from cold-vehicle starts during winter, which produce larger portions of EC in the exhaust; and (4) contributions from summertime forest fires in the surrounding mountains.

Ultrafine SOA[47,51] in relation to carbon levels is examined in Figure 4. N(84–407 nm) was reasonably correlated (r ~0.75 to 0.78) with BC concentration regardless of the season. However, N(3–84 nm) was not related to BC levels in summer, consistent with condensation of organic vapors on sulfuric acid nuclei formed by photochemical.

Mass Absorption Efficiencies

The 24-hr averaged b_{abs} from the MAAP, the 7-AE, and the photoacoustic analyzer were compared with filter-based IMPROVE EC to estimate σ_{abs} applicable to the Fresno aerosol. As shown in Figure 5, σ_{abs} is 5.5 m^2/g for MAAP (670 nm), 10 m^2/g for 7-AE (880 nm), and 2.3 m^2/g for the photoacoustic analyzer (1047 nm); these values are substantially different from the assumed values of 6.5, 16.6, and 5 m^2/g for the MAAP, 7-AE, and photoacoustic analyzer, respectively. The wavelength dependence of $b_{abs}(\lambda)$ and $\sigma_{abs}(\lambda)$ and the different exponents (α) in the $\lambda^{-\alpha}$ scaling factor, owing to changing particle compositions and shapes, lead to different relationships between BC and b_{abs}. Table 4 compares σ(670 nm) for λ^{-1}, λ^{-2} (typical of biomass burning[7]), and $\lambda^{-2.7}$ (found in ambient Denver, CO, aerosol by Moosmüller et al.[52]) for these instruments. The σ_{abs}(670 nm) values for the 7-AE and photoacoustic analyzer increase by a factor of 3 with α increasing from 1 to 2.7. At α = 2, σ_{abs}(670 nm) values for the 7-AE and photoacoustic analyzer differ only by 4 and 12% from the default σ_{abs}, respectively. With λ^{-2} scaling, the MAAP and photoacoustic analyzer had similar σ_{abs}(670 nm) values of 5.5 and 5.6 m^2/g, respectively.

Comparison of daily averaged 7-AE values with BC values at λ = 370 nm versus λ = 880 nm (Figure 6) shows that the built-in λ^{-1} scaling is consistent during summer, whereas a $\lambda^{-1.3}$ better approximates the situation during winter. As shown in Table 2, aethalometer (λ = 880 nm) and photoacoustic analyzer (λ = 1047 nm) BC values were correlated (r = 0.95–0.99) for winter and summer. Comparison between the aethalometer BC value at λ = 950 nm and photoacoustic BC yielded similar results. Absorption at longer wavelengths is less prone to deviation than

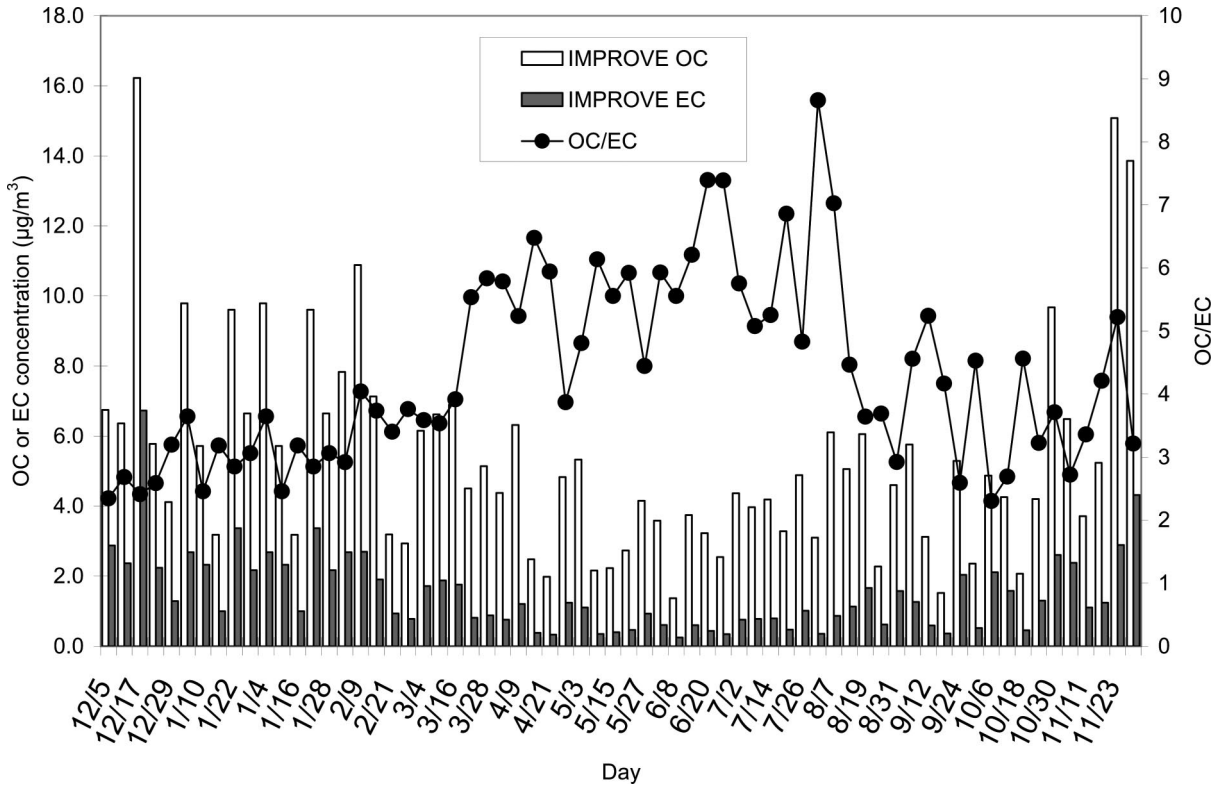

Figure 3. Twenty-four hour averages of OC and EC concentrations, and the OC/EC ratio measured by the DRI/OGC TOR carbon analyzer following the IMPROVE protocol for the period of December 2003 to November 2004.

absorption at shorter wavelengths. The assumed aethalometer σ_{abs}(880 nm) of 16.6 m^2/g may not apply because of a lack of consideration of multiple scattering effects in the aethalometer. This is evident in Figure 7a, as 7-AE b_{abs}(670 nm) ranges from 2.63 (winter) to 3.38 (summer) times higher than the MAAP b_{abs}, although they are highly correlated (r = 0.98–0.99). As shown in Figure 7b, MAAP b_{abs} is 1.52 (winter) to 1.23 (summer) times higher than the photoacoustic b_{abs}, still with a high correlation of 0.96–0.99. Better regression slopes of 1.33 (winter) and 1.07 (summer) can be obtained for the MAAP versus photoacoustic comparison if α = 1.3 is used (determined by Schnaiter et al.[25] with diesel exhaust).

As noted earlier, the σ_{abs}(1047 nm) of 5 m^2/g for the photoacoustic analyzer was derived from simultaneous measurements of diesel exhaust by IMPROVE EC.[40] As shown in Tables 2 and 3, this is not an appropriate assumption for the Fresno summer or winter aerosols. The 5 m^2/g assumption is also inconsistent with the suggestion of Bond and Bergstrom[14] cited above for fresh particle emissions, which yields a 1 SD range of 3.3–4.6 m^2/g at λ = 1047 nm assuming a λ^{-1} scaling. This range is 1.7–2.5 m^2/g with a λ^{-2} scaling. An α between 1 and 2 might be more appropriate for mixed and aged aerosol such as that found at the Fresno Supersite.

It is evident that wavelength has an important effect on the conversion of b_{abs} to BC. BC values obtained at different wavelengths might be useful in separating vegetative burning from other sources by use of receptor models.[53–55]

Diurnal Variations of the Single Scattering Albedo

The single scattering albedo ($\omega = b_{scat}/[b_{scat} + b_{abs}]$) was calculated using b_{scat}(530 nm) values obtained by nephelometer and b_{abs} (scaled from 1047 to 530 nm assuming λ^{-1}) values obtained by the photoacoustic analyzer. Higher values of daily ω were observed in winter (0.89) than in summer (0.80), consistent with particles containing more scattering species during winter. Higher RH in winter increases b_{scat} and therefore contributes to the higher ω. As shown in Figure 8, in winter the lowest ω occurred during the early morning rush hour of ~7:00 a.m. Pacific Standard Time (PST) and at ~8:00 p.m. PST. In summer, the lowest ω occurred at ~6:00 a.m. and at 7:00 p.m. PST. Times of low ω coincided with the peak b_{abs} occurrences. Although the evening b_{abs} peak was higher and broader than the morning b_{abs} peak in winter, the values of ω were comparable during both seasons.

Diurnal Variations of BC Concentrations

As shown in Figure 9, the dual peaks for hourly average BC levels were 7:00–8:00 a.m. PST and 8:00–10:00 p.m. PST in winter. The large evening peak persisted through midnight and early morning of the following day. This is consistent with increased emissions from morning and evening traffic and from RWC emissions that accumulate under the surface inversion during winter evenings.[50] In summer, the morning BC peak occurred at ~6:00 a.m. PST with a small evening peak at ~8:00 p.m. PST. The times of the peak concentrations of PAH, NO_x, and CO coincided

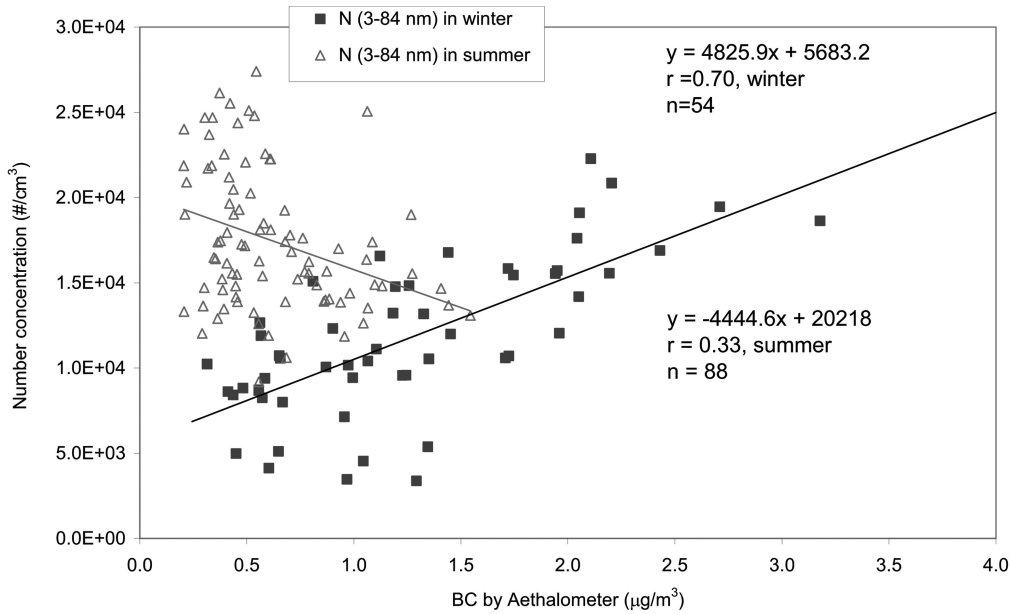

(a)

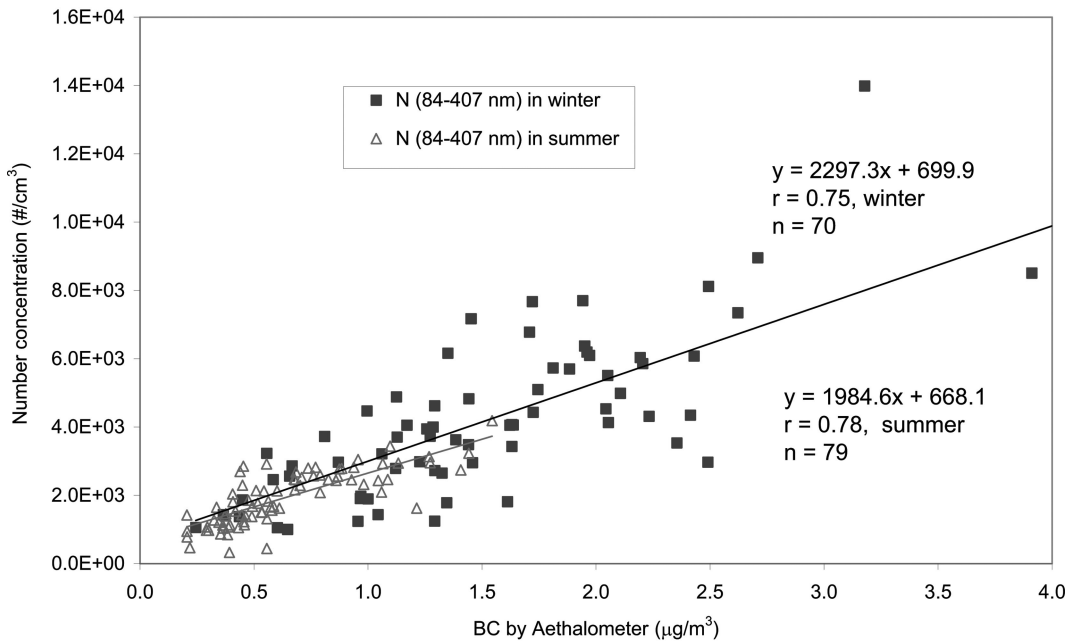

(b)

Figure 4. Particle number concentrations in the size ranges of (a) 3–84 nm and (b) 84–407 nm by the SMPS versus BC concentration by 7-AE (λ = 880 nm) for daily average in winter (December 2003 to February 2004) and summer (June to August 2004).

with the BC peak, and these followed similar seasonal patterns (i.e., the evening peak was more dominant in winter than in summer). The morning $PM_{2.5}$ peak lagged behind the BC peak by 1 to 2 hr. $PM_{2.5}$ NO_3^- levels increased after 7:00 a.m. PST in winter. The time for increasing NO_3^- is consistent with times for increasing temperature and decreasing BC, NO_x, and CO. This is consistent with NO_3^- formation above the surface layer with downward mixing when the layers couple.[50] During summer, the NO_3^- concentrations increased until ~8:00 a.m. PST and then decreased until the late afternoon, consistent with evaporation as temperatures increase.

CONCLUSIONS

$PM_{2.5}$ BC or EC concentrations at the Fresno Supersite are higher in winter than in summer. This is consistent with primary combustion emissions from traffic and home heating that accumulate under a shallow surface layer during winter nights. Similar seasonal patterns are observed for $PM_{2.5}$ mass, NO_3^-, PAH, NO_x, CO, ω, and

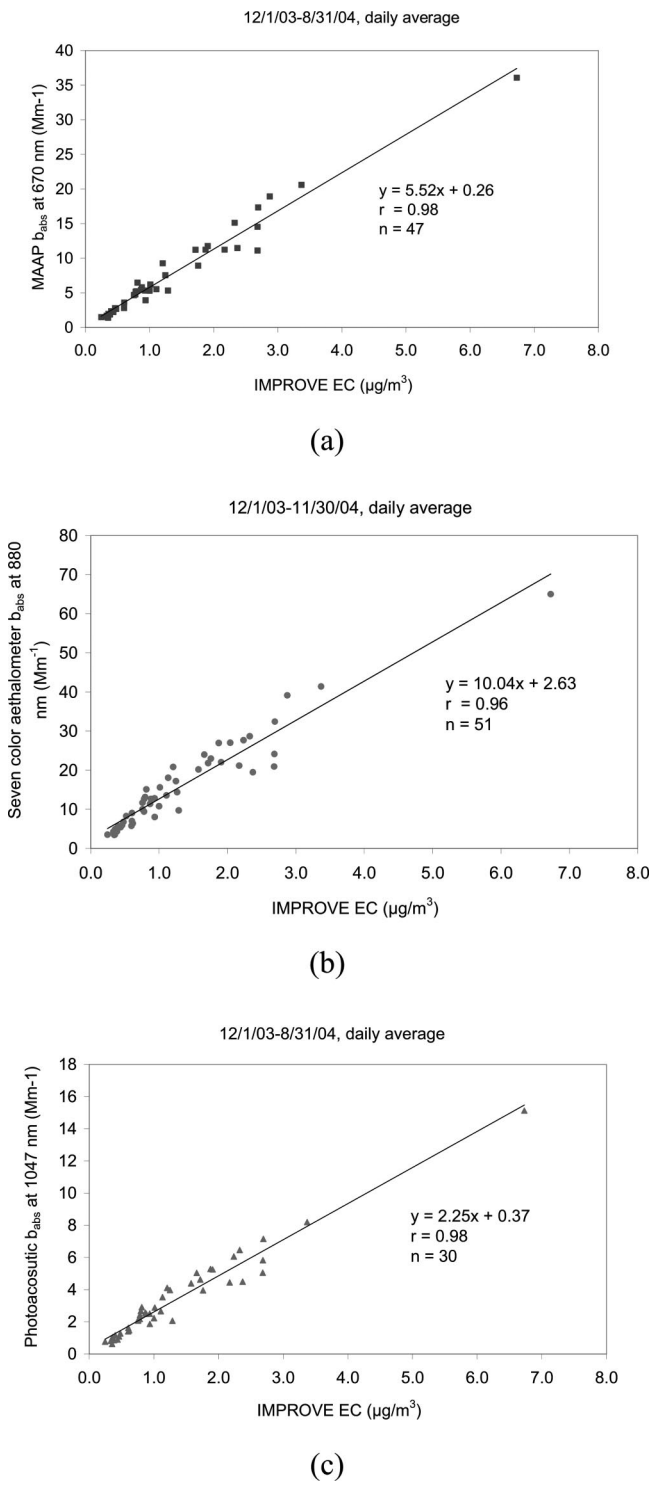

Figure 5. Mass absorption efficiencies calculated with (a) MAAP (λ = 670 nm), (b) 7-AE (λ = 880 nm), and (c) photoacoustic analyzer (λ = 1047 nm) versus IMPROVE EC concentrations. The aethalometer light attenuation is reported as light absorption without any calibration factor.

number concentration for particles in the accumulation mode [N(84–407 nm)]. The diurnal pattern of BC is consistent with those for PAH, NO_x, and CO, indicating that primary combustion emissions accumulate during early morning and night and decrease as the mixing layer increases, especially during the winter. Higher ratios of BC at λ = 370 nm to BC at λ = 880 nm occur during the winter, consistent with a larger contribution from RWC that absorbs more in the UV part of the spectrum. The number of ultrafine particles (3–84 nm) and the OC/EC ratio are lower during winter than summer, both of which are consistent with formation of SOA through vapor condensation.

Compared with IMPROVE EC, mass absorption efficiencies for Fresno are 5.5 m^2/g for the MAAP at 670 nm, 10 m^2/g for the aethalometer at 880 nm, and 2.3 m^2/g for the photoacoustic analyzer at 1047 nm. These differ from the assumed values of 6.5 m^2/g for the MAAP, 16.6 m^2/g for the aethalometer, and 5 m^2/g for the photoacoustic analyzer.

Intercomparisons show good correlations among all BC or EC measures except for the R&P 5400 EC, but with slopes ranging from 0.2 to 2. The degree of comparability differed between winter and summer, reinforcing the difference in aerosol composition with the season; σ_{abs} does not scale as λ^{-1} at Fresno.

ACKNOWLEDGMENTS

The Fresno Supersite is a cooperative effort between the California Air Resources Board (ARB) and the DRI. Sponsorship is provided by the U.S. Environmental Protection Agency through the Cooperative Institute for Atmospheric Sciences and Terrestrial Applications (CIASTA) of the National Oceanic and Atmospheric Administration and the California Regional Particulate Air Quality Study (CRPAQS) under the management of Ms. Karen Magliano of the ARB. This work was partially supported by U.S. Environmental Protection Agency STAR Grant No. RD-83108601-0. The conclusions are those of the authors and do not necessarily reflect the views of the sponsoring agencies. Any mention of commercially available products and supplies does not constitute an endorsement of those products and supplies. The authors thank Scott Scheller of the ARB and Dr. Susanne Hering of Aerosol Dynamics, Inc., for their efforts in maintaining the monitoring instruments. Dr. John Bowen, Steve Kohl, and Ms. Barbara Hinsvark of DRI assisted in field coordination, laboratory operations, and data processing of Supersite measurements. Ms. Jo Gerrard and Tim Richard of DRI assisted with assembling and editing the manuscript.

REFERENCES

1. Watson, J.G. Visibility: Science and Regulation; *J. Air & Waste Manage. Assoc.* **2002,** *52,* 628-713.
2. Watson, J.G. Visibility: Science and Regulation - A Summary of the 2002 Critical Review; *EM* **2002**, *8,* 36-43.
3. Jacobson, M.Z. Control of Fossil-Fuel Particulate Black Carbon plus Organic Matter, Possibly the Most Effective Method of Slowing Global Warming; *J. Geophys. Res.* **2002**, *107*, ACH 16-1-ACH 16-22.
4. Vedal, S. Critical Review - Ambient Particles and Health: Lines That Divide; *J. Air & Waste Manage. Assoc.* **1997**, *47,* 551-581.
5. Watson, J.G.; Chow, J.C.; Chen, L.-W.A. Summary of Organic and Elemental Carbon/Black Carbon Analysis Methods and Intercomparisons; *Aerosol Air Qual. Res.* **2005**, *1,* 69-102.
6. Horvath, H. Atmospheric Light Absorption - A Review; *Atmos. Environ.* **1993**, *27A*, 293-317.
7. Kirchstetter, T.W.; Novakov, T.; Hobbs, P.V. Evidence That the Spectral Dependence of Light Absorption by Aerosols Is Affected by Organic Carbon; *J. Geophys. Res.* **2004**, *109*, D21208.
8. Bond, T.C.; Anderson, T.L.; Campbell, D.E. Calibration and Intercomparison of Filter-based Measurements of Visible Light Absorption by Aerosols; *Aerosol Sci. Technol.* **1999**, *30,* 582-600.

Table 4. Comparisons of assumed absorption coefficients with measured values and wavelength-corrected absorption efficiencies.

Instruments	Assumed Absorption Efficiency (m^2/g)[a]	Fresno Absorption Efficiency at Instrument λ (m^2/g)[b]	Estimated Absorption Efficiency		
			Scaled by λ^{-1} to 670 nm[c]	Scaled by $\lambda^{-2.0}$ to 670 nm	Scaled by $\lambda^{-2.7}$ to 670 nm
MAAP (670 nm)	6.5	5.5	5.5	5.5	5.5
7-AE (880 nm)	16.6[d]	10.0	13.1	17.3	27.4
Photoacoustic analyzer (1047 nm)	5.0	2.3	3.5	5.6	11.7

Notes: [a]Conversion factors assumed to convert light absorption (for MAAP and photoacoustic analyzer) or light attenuation (for 7-AE) to BC concentration; [b]Regression slope from light absorption (for MAAP and photoacoustic analyzer) or light attenuation (for 7-AE) vs IMPROVE EC concentration; [c]Based on the Angstrom Power Law with different exponents ($b_{abs} \sim \lambda^{-\alpha}$): $\alpha = 1$ by Angstrom Power Law; $\alpha = 2$ by Kirchstetter et al.[7]; and $\alpha = 2.7$ by Moosmüller et al.[52]; [d]Based on 14,625/λ at 880 nm; the aethalometer light attenuation (Mm^{-1}) is reported as light absorption without any calibration factor in this study.

9. Lindberg, J.D.; Douglass, R.E.; Garvey, D.M. Atmospheric Particulate Absorption and Black Carbon Measurement; *Appl. Opt.* **1999**, *38,* 2369-2376.
10. Petzold, A.; Schönlinner, M. Multi-angle Absorption Photometry - A New Method for the Measurement of Aerosol Light Absorption and Atmospheric Black Carbon; *J. Aerosol Sci.* **2004**, *35,* 421-441.
11. Fuller, K.A.; Malm, W.C.; Kreidenweis, S.M. Effects of Mixing on Extinction by Carbonaceous Particles; *J. Geophys. Res.* **1999**, *104,* 15941-15954.
12. Martins, J.V.; Artaxo, P.; Liousse, C.; Reid, J.S.; Hobbs, P.V.; Kaufman, Y.J. Effects of Black Carbon Content, Particle Size, and Mixing on Light Absorption by Aerosols from Biomass Burning in Brazil; *J. Geophys. Res.* **1998**, *103,* 32041-32050.
13. Liousse, C.; Cachier, H.; Jennings, S.G. Optical and Thermal Measurements of Black Carbon Aerosol Content in Different Environments: Variation of the Specific Attenuation Cross-section, Sigma (σ); *Atmos. Environ.* **1993**, *27A,* 1203-1211.
14. Bond, T.C.; Bergstrom, R.W. Light Absorption by Carbonaceous Particles: An Investigative Review; *Aerosol Sci. Technol.* **2006**, *40,* 27-67.
15. Chow, J.C.; Watson, J.G. $PM_{2.5}$ Carbonate Concentrations at Regionally Representative Interagency Monitoring of Protected Visual Environment Sites; *J. Geophys. Res.* **2002**, *107,* ICC 6-1-ICC 6-9.
16. Cao, J.J.; Lee, S.C.; Zhang, X.Y.; Chow, J.C.; An, Z.S.; Ho, K.F.; Watson, J.G.; Fung, K.K.; Wang, Y.Q.; Shen, Z.X. Characterization of Airborne Carbonate over a Site near Asian Dust Source Regions during Spring 2002 and Its Climatic and Environmental Significance; *J. Geophys. Res.* **2005**, *110,* 1-8.
17. Chow, J.C.; Watson, J.G.; Chen, L.-W.A.; Arnott, W.P.; Moosmüller, H.; Fung, K.K. Equivalence of Elemental Carbon by Thermal/Optical Reflectance and Transmittance with Different Temperature Protocols; *Environ. Sci. Technol.* **2004**, *38,* 4414-4422.
18. Chen, L.-W.A.; Chow, J.C.; Watson, J.G.; Moosmüller, H.; Arnott, W.P. Modeling Reflectance and Transmittance of Quartz-Fiber Filter Samples Containing Elemental Carbon Particles: Implications for Thermal/Optical Analysis; *J. Aerosol. Sci.* **2004**, *35,* 765-780.
19. Currie, L.A.; Benner, B.A., Jr.; Cachier, H.; Cary, R.; Chow, J.C.; Druffel, E.R.M.; Eglinton, T.I.; Gustafsson, Ö.; Hartmann, P.C.; Hedges, J.I.; Kessler, J.D.; Kirchstetter, T.W.; Klinedinst, D.B.; Klouda, G.A.; Marolf, J.V.; Masiello, C.A.; Novakov, T.; Pearson, A.; Prentice, K.M.; Puxbaum, H.; Quinn, J.G.; Reddy, C.M.; Schmid, H.; Slater, J.F.; Watson, J.G.; Wise, S.A. A Critical Evaluation of Interlaboratory Data on Total, Elemental, and Isotopic Carbon in the Carbonaceous Particle Reference Material, NIST SRM 1649a; *J. Res. Natl. Bur. Stand. (U.S.)* **2002**, *107,* 279-298.
20. Arnott, W.P.; Moosmüller, H.; Rogers, C.F.; Jin, T.; Bruch, R. Photoacoustic Spectrometer for Measuring Light Absorption by Aerosol: Instrument Description; *Atmos. Environ.* **1999**, *33,* 2845-2852.
21. Bell, A.G. Production of Sound by Radiant Energy; *The Manufacturer and Builder,* **1881**, *15,* 156-158.
22. Bruce, C.W.; Pinnick, R.G. *In-Situ* Measurements of Aerosol Absorption with a Resonant CW Laser Spectrophone; *Appl. Opt.* **1977**, *16,* 1762-1764.
23. Saathoff, H.; Naumann, K.H.; Schnaiter, M.; Schöck, W.; Weingartner, E.; Baltensperger, U.; Krämer, L.; Bozoki, Z.; Pöschl, U.; Niessner, R.; Schurath, U. Carbon Mass Determinations during the AIDA Soot Aerosol Campaign 1999; *J. Aerosol Sci.* **2003**, *34,* 1399-1420.
24. Saathoff, H.; Moehler, O.; Schurath, U.; Kamm, S.; Dippel, B.; Mihelcic, D. The AIDA Soot Aerosol Characterisation Campaign 1999; *J. Aerosol Sci.* **2003**, *34,* 1277-1296.
25. Schnaiter, M.; Horvath, H.; Mohler, O.; Naumann, K.H.; Saathoff, H.; Schock, O.W. UV-VIS-NIR Spectral Optical Properties of Soot and Soot-containing Aerosols; *J. Aerosol. Sci.* **2003**, *34,* 1421-1444.
26. Sheridan, P.J.; Arnott, W.P.; Ogren, J.A.; Andrews, E.; Atkinson, D.B.; Covert, D.S.; Moosmüller, H.; Petzold, A.; Schmid, B.; Strawa, A.W.; Varma, R.; Virkkula, A. The Reno Aerosol Optics Study: An Evaluation of Aerosol Absorption Measurement Methods; *Aerosol. Sci. Technol.* **2005**, *39,* 1-16.
27. Watson, J.G.; Chow, J.C.; Bowen, J.L.; Lowenthal, D.H.; Hering, S.; Ouchida, P.; Oslund, W. Air Quality Measurements from the Fresno Supersite; *J. Air & Waste Manage. Assoc.* **2000**, *50,* 1321-1334.
28. Watson, J.G.; Chow, J.C. Comparison and Evaluation of In-Situ and Filter Carbon Measurements at the Fresno Supersite; *J. Geophys. Res.* **2002**, *107,* ICC 3-1-ICC 3-15.
29. Chow, J.C.; Watson, J.G.; Lowenthal, D.H.; Solomon, P.A.; Magliano, K.L.; Ziman, S.D.; Richards, L.W. PM_{10} and $PM_{2.5}$ Compositions in California's San Joaquin Valley; *Aerosol. Sci. Technol.* **1993**, *18,* 105-128.
30. Chow, J.C.; Chen, L.-W.A.; Watson, J.G.; Lowenthal, D.H.; Magliano, K.; Turkiewicz, K.; Lehrman, D. $PM_{2.5}$ Chemical Composition and Spatiotemporal Variability during the California Regional $PM_{10}/PM_{2.5}$ Air Quality Study (CRPAQS); *J. Geophys. Res.* **2006**, in press.
31. Hansen, A.D.A.; Rosen, H.; Novakov, T. The Aethalometer - An Instrument for the Real-Time Measurement of Optical Absorption by Aerosol Particles; *Sci. Total Environ.* **1984**, *36,* 191-196.
32. Arnott, W.P.; Hamasha, K.; Moosmüller, H.; Sheridan, P.J.; Ogren, J.A. Towards Aerosol Light-Absorption Measurements with a 7-Wavelength Aethalometer: Evaluation with a Photoacoustic Instrument and 3-Wavelength Nephelometer; *Aerosol Sci. Technol.* **2005**, *39,* 17-29.
33. Petzold, A.; Kramer, H.; Schönlinner, M. Continuous Measurement of Atmospheric Black Carbon Using a Multi-angle Absorption Photometer; *Environ. Sci. Pollut. Res.* **2002**, *Special Issue,* 478-82.
34. Petzold, A.; Schloesser, H.; Sheridan, P.J.; Arnott, W.P.; Ogren, J.A.; Virkkula, A. Evaluation of Multiangle Absorption Photometry for Measuring Aerosol Light Absorption; *Aerosol Sci. Technol.* **2005**, *39,* 40-51.
35. VDI Measurement of Soot (Ambient Air)—Thermographic Determination of Elemental Carbon after Thermal Desorption of Organic Carbon; Berein Deutscher: Dusseldorf, Germany, 1999, (2465 Part 2).
36. Schmid, H.P.; Laskus, L.; Abraham, H.J.; Baltensperger, U.; Lavanchy, V.M.H.; Bizjak, M.; Burba, P.; Cachier, H.; Crow, D.; Chow, J.C.; Gnauk, T.; Even, A.; ten Brink, H.M.; Giesen, K.P.; Hitzenberger, R.; Hueglin, C.; Maenhaut, W.; Pio, C.A.; Puttock, J.; Putaud, J.P.; Toom-Sauntry, D.; Puxbaum, H. Results of the "Carbon Conference" International Aerosol Carbon Round Robin Test: Stage 1; *Atmos. Environ.* **2001**, *35,* 2111-2121.
37. Chow, J.C.; Watson, J.G.; Pritchett, L.C.; Pierson, W.R.; Frazier, C.A.; Purcell, R.G. The DRI Thermal/Optical Reflectance Carbon Analysis System: Description, Evaluation and Applications in U.S. Air Quality Studies; *Atmos. Environ.* **1993**, *27A,* 1185-1201.
38. Chow, J.C.; Watson, J.G.; Crow, D.; Lowenthal, D.H.; Merrifield, T.M. Comparison of IMPROVE and NIOSH Carbon Measurements; *Aerosol Sci. Technol.* **2001**, *34,* 23-34.
39. Arnott, W.P.; Moosmüller, H.; Sheridan, P.J.; Ogren, J.A.; Raspet, R.; Slaton, W.V.; Hand, J.L.; Kreidenweis, S.M.; Collett, J.L., Jr. Photoacoustic and Filter-based Ambient Aerosol Light Absorption Measurements: Instrument Comparison and the Role of Relative Humidity; *J. Geophys. Res.* **2003**, *108,* AAC 15-1-AAC 15-11.
40. Arnott, W.P.; Zielinska, B.; Rogers, C.F.; Sagebiel, J.; Park, K.; Chow, J.C.; Moosmüller, H.; Watson, J.G.; Kelly, K.; Wagner, D.; Sarofim, A.; Lighty, J.; Palmer, G. Evaluation of 1047 nm Photoacoustic Instruments and Photoelectric Aerosol Sensors in Source-Sampling of Black Carbon Aerosol and Particle Bound PAH's from Gasoline and Diesel Powered Vehicles; *Environ. Sci. Technol.* **2005**, *39,* 5398-5406.
41. Bae, M.S.; Schauer, J.J.; Deminter, J.T.; Turner, J.R.; Smith, D.; Cary, R.A. Validation of a Semi-continuous Instrument for Elemental Carbon and Organic Carbon Using a Thermal-Optical Method; *Atmos. Environ.* **2004**, *38,* 2885-2893.

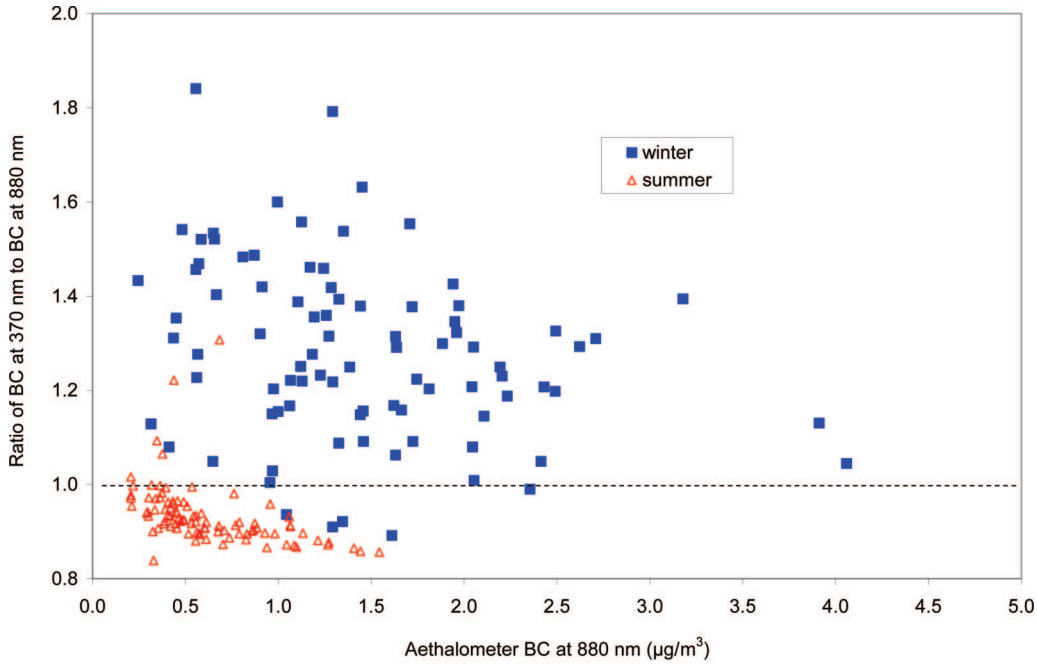

(a)

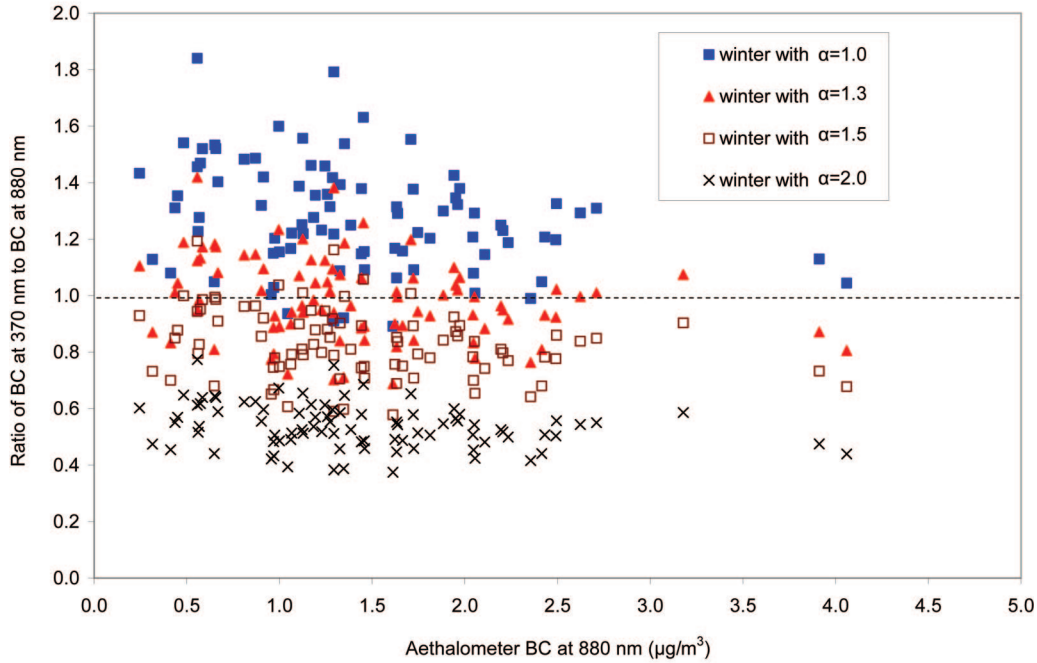

(b)

Figure 6. Ratio of daily averaged BC at the wavelength of 370 nm versus 880 nm as a function of the 7-AE BC concentration at $\lambda = 880$ nm in (a) winter (December 2003 to February 2004) and in summer (June to August 2004), and (b) in winter with different exponents (α) in the $\gamma-\alpha$ scaling factor.

42. Jeong, C.H.; Hopke, P.K.; Kim, E.; Lee, D.W. The Comparison between Thermal-Optical Transmittance Elemental Carbon and Aethalometer Black Carbon Measured at Multiple Monitoring Sites; *Atmos. Environ.* **2004**, *38,* 5193-5204.
43. Rupprecht, E.G.; Patashnick, H.; Beeson, D.E.; Green, R.E.; Meyer, M.B. A New Automated Monitor for the Measurement of Particulate Carbon in the Atmosphere. In *Proceedings, Particulate Matter: Health and Regulatory Issues,* April 4–6, 1995, Cooper, J.A. and Grant, L.D., Eds.; Air and Waste Management Association: Pittsburgh, PA, 1995, pp. 262-267.
44. Burtscher, H.; Schmidt-Ott, A. In Situ Measurement of Adsorption and Condensation of a Polyaromatic Hydrocarbon on Ultrafine Carbon

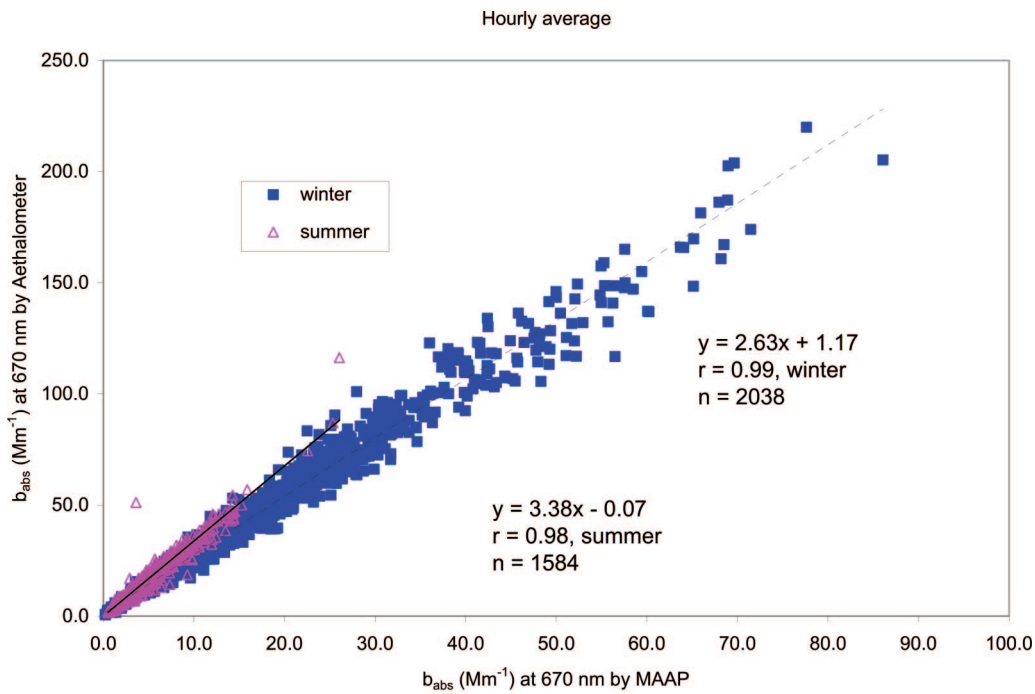

(a)

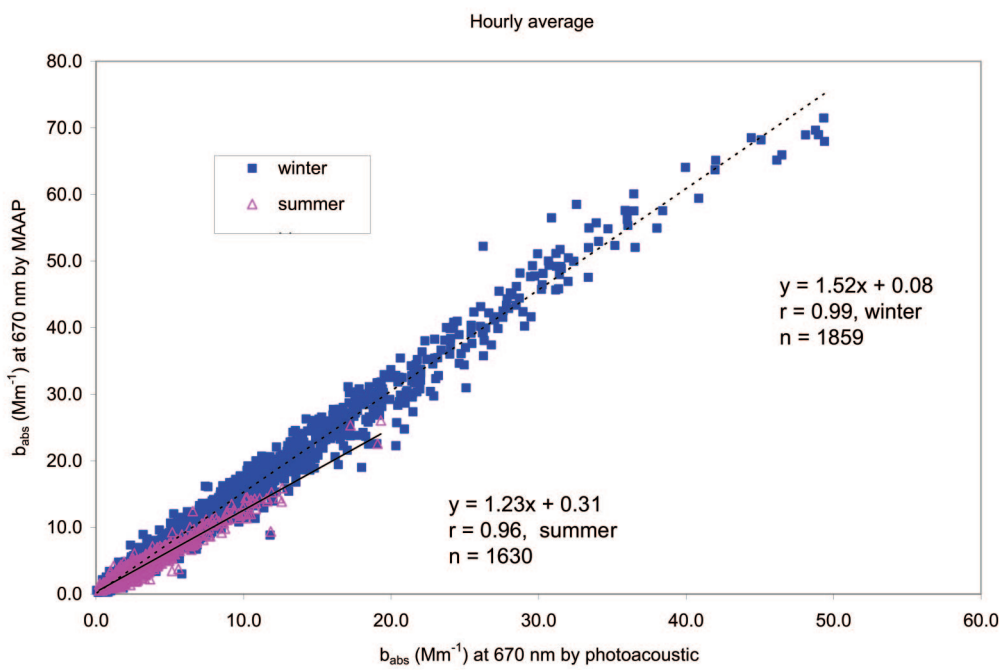

(b)

Figure 7. Hourly averaged (a) b_{abs} by 7-AE versus b_{abs} by MAAP at $\lambda = 670$ nm and (b) MAAP b_{abs} vs. photoacoustic b_{abs} at $\lambda = 670$ nm in winter (December 2003 to February 2004) and summer (June to August 2004)

Particles by Measurement of Photoemission; *J. Aerosol Sci.* **1986**, *18,* 699.

45. United States Environmental Protection Agency. Revised Requirements for Designation of Reference and Equivalent Methods for $PM_{2.5}$ and Ambient Air Surveillance for Particulate Matter—Final Rule; *Fed. Regist.* **1997**, *138,* 38763-38854.
46. Chow, J.C.; Watson, J.G.; Lowenthal, D.H.; Chen, L.-W.A.; Magliano, K. Particulate Carbon Measurements in California's San Joaquin Valley; *Chemosphere,* **2006**, *62,* 337-348.
47. Watson, J.G.; Chow, J.C.; Lowenthal, D.H.; Kreisberg, N.; Hering, S.V.; Stolzenburg, M.R. Variations of Nanoparticle Concentrations at the Fresno Supersite. *Sci. Total Environ.* **2006**, *358,* 178-187.

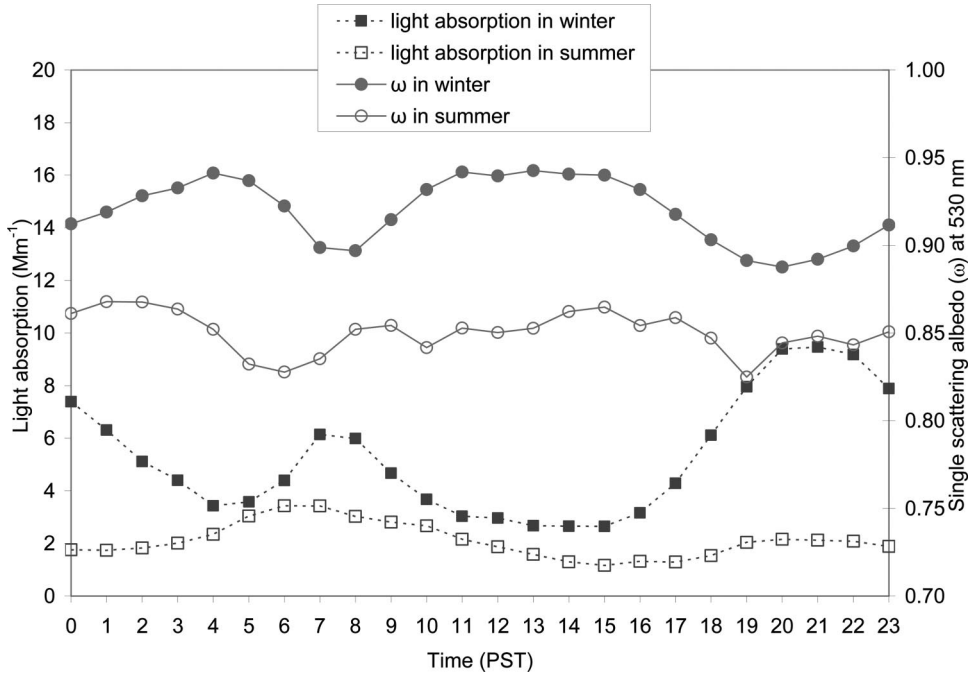

Figure 8. Diurnal variation of the single scattering albedo (ω) calculated by use of particle light scattering (b_{scat}) from the nephelometer (λ = 530 nm) and light absorption (b_{abs}) from the photoacoustic analyzer (λ = 1047 nm) averaged by the time of day in winter (December 2003 to February 2004) and summer (June to August 2004).

48. Richards, L.W.; Lehrman, D.E.; Weiss, R.E.; Bush, D.; Watson, J.G.; McDade, C.E.; Magliano, K. Light scattering measurements during the California Regional $PM_{10}/PM_{2.5}$ Air Quality Study. In *Proceedings, International Specialty Conference on Regional Haze and Global Radiation Balance—Aerosol Measurements and Models: Closure, Reconciliation and Evaluation*, Air & Waste Management Association/American Geophysical Union: Pittsburgh, PA/Washington, DC, 2001.
49. Patashnick, H.; Rupprecht, E.G. Continuous PM_{10} Measurements Using the Tapered Element Oscillating Microbalance; *J. Air & Waste Manage. Assoc.* **1991**, *41,* 1079-1083.
50. Watson, J.G.; Chow, J.C. A Wintertime $PM_{2.5}$ Episode at the Fresno, CA, Supersite; *Atmos. Environ.* **2002**, *36,* 465-475.
51. Watson, J.G.; Chow, J.C.; Park, K.; Lowenthal, D.H. Nanoparticle and Ultrafine Particle Events at the Fresno Supersite; *J. Air & Waste Manage. Assoc.* **2006**, *55,* 417-430.
52. Moosmüller, H.; Arnott, W.P.; Rogers, C.F.; Chow, J.C.; Frazier, C.A.; Sherman, L.E.; Dietrich, D.L. Photoacoustic and Filter Measurements Related to Aerosol Light Absorption during the Northern Front Range Air Quality Study (Colorado 1996/1997); *J. Geophys. Res.* **1998**, *103*, 28149-28157.
53. Watson, J.G.; Chow, J.C.; Houck, J.E. $PM_{2.5}$ Chemical Source Profiles for Vehicle Exhaust, Vegetative Burning, Geological Material, and Coal Burning in Northwestern Colorado during 1995; *Chemosphere,* **2001**, *43,* 1141-1151.
54. Watson, J.G.; Zhu, T.; Chow, J.C.; Engelbrecht, J.P.; Fujita, E.M.; Wilson, W.E. Receptor Modeling Application Framework for Particle Source Apportionment; *Chemosphere,* **2002**, *49,* 1093-1136.
55. Watson, J.G.; Chow, J.C. Receptor Models for Air Quality Management; *EM,* **2004,** *10,* 27-36.

About the Authors

Kihong Park was formerly an assistant research professor at the Desert Research Institute (DRI) and is currently an assistant professor at the Gwangju Institute of Science and Technology. Judith C. Chow and John G. Watson are research professors, Dana Trimble is an associate research scientist, and Prakash Doraiswamy is a post doctoral research associate at DRI. W. Pat Arnott is an associate professor at the University of Nevada, Reno. Kenneth R. Stroud is chief of the Air Quality Surveillance Branch, Kenneth Bowers is an air pollution specialist, and Richard D. Bode is chief of the Health and Exposure Assessment Branch of the California Air Resources Board. Andre Petzold is head of the Atmosphereic Group at the Instutue of Atmoshperic Physics (Deutsches Zentrum fur Luft - und Raumfahrt Oberpfaffenhofen, Institute fur Physic der Atmosphare). Anthonty D. A. Hansen is a staff scientist for the Engineering Division of Lawrence Berkeley National Laboratory. Address correspondence to: Judith C. Chow, Division of Atmospheric Sciences, Desert Research Institute, 2215 Raggio Parkway, Reno, NV 89512; phone: +1-775-674-7050; fax: +1-775-674-7009; e-mail: judy.chow@dri.edu.

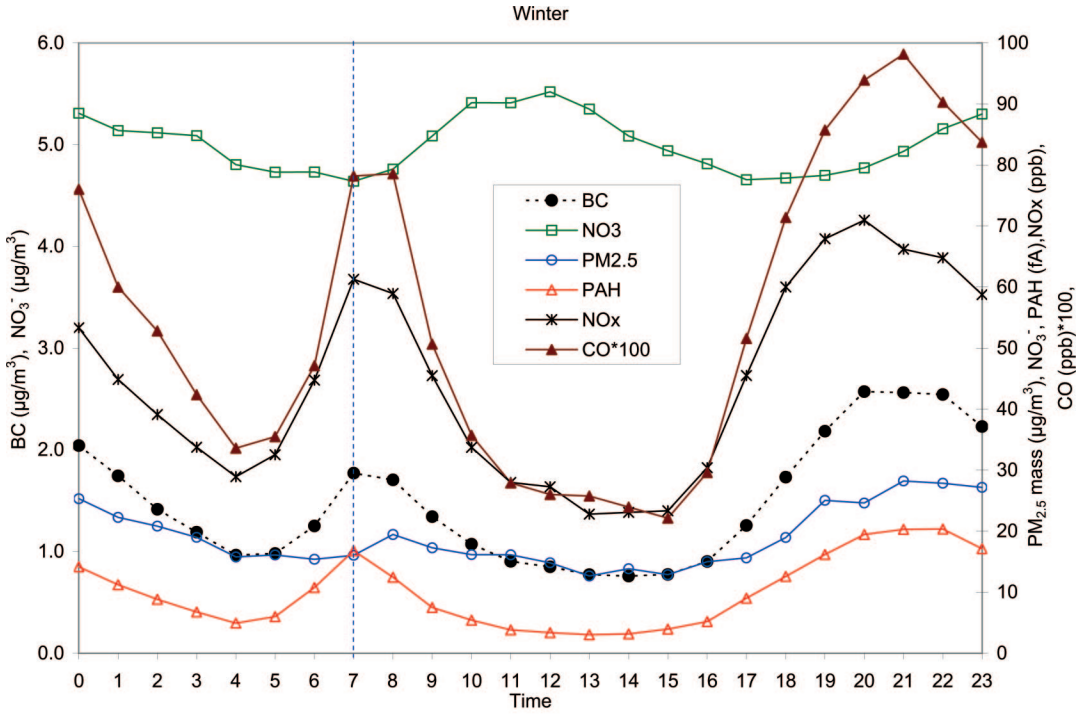

(a)

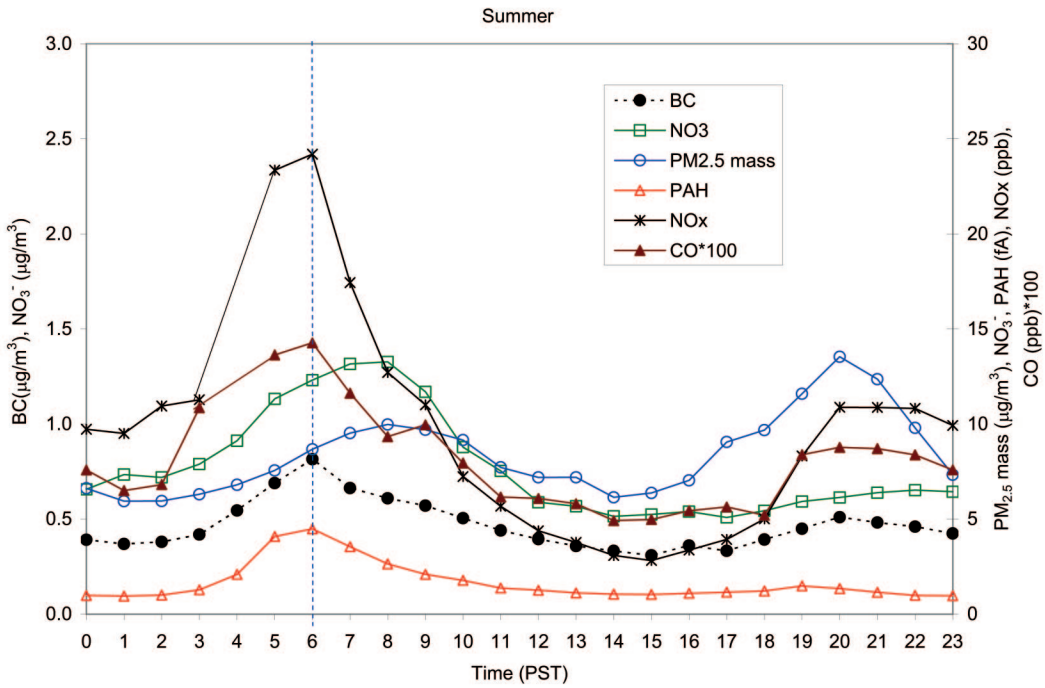

(b)

Figure 9. Diurnal variations of BC, NO_3^-, $PM_{2.5}$ mass, particle-bound PAHs, NO_x, and CO averaged by the time of day for (a) winter (December 2003 to February 2004) and (b) summer (June to August 2004)

Copyright of Journal of the Air & Waste Management Association (1995) is the property of Air & Waste Management Association and its content may not be copied or emailed to multiple sites or posted to a listserv without the copyright holder's express written permission. However, users may print, download, or email articles for individual use.